J Petrol Explor Prod Technol

https://doi.org/10.1007/s13202-026-02144-6

Article in Press

Site specific geophysical-geotechnical integration: correlating ERT and SPT for subsurface characterisation

Received: 4 October 2025

Accepted: 4 April 2026

Published online: 15 April 2026

Cite this article as: Najar I.A., Ahmadi R., Mourad R. *et al.* Site specific geophysical-geotechnical integration: correlating ERT and SPT for subsurface characterisation. *J Petrol Explor Prod Technol* (2026). https://doi.org/10.1007/s13202-026-02144-6

Imtiyaz Akbar Najar, Raudhah Ahmadi, Raghad Mourad, Nadeem A Khan, Retinder Kour, Yunika Kirana Abdul Khalik, ., Dayangku Salma Awang Ismail, ., Haythem Dinar, Nouh Rebouh, Azrin Ahmad & Shaiza Asif

Site Specific Geophysical-Geotechnical Integration: Correlating ERT and SPT for Subsurface Characterisation

Imtiyaz Akbar Najar[1]*, Raudhah Ahmadi[1]*, Raghad Mourad[2], Nadeem A Khan[3], Retinder Kour[4], Yunika Kirana Abdul Khalik[1], Dayangku Salma Awang Ismail[1], Haythem Dinar[5], Nouh Rebouh[5], Azrin Ahmad[6], Shaiza Asif[1]

[1]Faculty of Engineering, Universiti Malaysia Sarawak, 94300, Kota Samarahan, Sarawak, Malaysia

[2]Department of Architecture, College of Architecture, Art and Design, Ajman University, Ajman, United Arab Emirates

[3]Civil Engineering Department, College of Engineering, King Khalid University, Abha, 61421, Saudi Arabia

[4]Interdisciplinary Centre for Water Research, Indian Institute of Science, Bangalore - 560012. India

[5]Centre de Recherche en Aménagement de Territoire (CRAT), Campus Zouaghi Slimane, Route de Ain el Bey, 25000, Constantine, Algérie

[6]Maltimur Aktif Unggul JV Sdn. Bhd. Kuching, Sarawak, Malaysia

*Corresponding author: 20010158@siswa.unimas.my; araudhah@unimas.my

Site Specific Geophysical-Geotechnical Integration: Correlating ERT and SPT for Subsurface Characterisation

Abstract

Subsurface investigations are critical for infrastructure development in the Lubok Antu region of Sarawak, Malaysia due to its complex geological conditions and seismic risk. Conventional geotechnical site investigation, such as standard penetration test (SPT) is accurate but discrete, costly, and limited in spatial coverage. This study established robust, site-specific correlations between electrical resistivity tomography (ERT) and key geotechnical parameters to enable rapid, cost-effective subsurface characterisation. ERT surveys and SPT boreholes were conducted at nine locations with a maximum depth of 30 meters. Soil resistivity (ρ) was correlated with SPT - N values, shear wave velocity (V_s) derived from empirical relationships, and laboratory measured moisture content (□) and plasticity index (PI). A strong nonlinear correlation was observed between ρ and □ (R^2=0.74), while moderate linear correlations were found for V_s (R^2=0.62) and SPT - N (R^2=0.55). The results demonstrate that ERT can effectively estimate geotechnical properties, offering a practical tool for preliminary site assessment that reduces reliance on extensive and expensive drilling programs. This study offers a novel approach for geotechnical investigation in Lubok Antu, reducing the reliance on extensive drilling programs and improving the efficiency of subsurface

investigations. The developed correlations are particular valuable for seismic hazard assessment and foundation designs in this tectonically active region. Subsurface investigation is essential in geotechnical and earthquake engineering.

Keywords: Electrical resistivity, ERT,SPT - N, shear wave velocity, soil moisture content.

1. Introduction

Subsurface investigation is crucial for infrastructure development in Lubok Antu, Malaysia, given its complex geological conditions and potential seismic risks (Zhao et al., 2021). Accurate geotechnical and geophysical data are vital for designing safe infrastructure in this tectonically active region. However, traditional geotechnical methods like the Standard Penetration Test (SPT - N), provides reliable soil property measurements, its high cost and discrete nature limit its effectiveness for large-area characterisation (Hassan et al., 2024). Given the highly complex and variable subsurface conditions, achieving a consistent and accurate understanding of soil and rock properties remains challenging (Hossain et al., 2018). To overcome these limitations, non-destructive geophysical methods like electrical resistivity tomography (ERT) are increasingly used to complement direct sampling. ERT provides continuous subsurface profiles quickly and cost-effectively (Al-Heety et al., 2021), induced polarisation (Kemna et al., 2012), seismic refraction (Hunter et al., 2022), magnetic surveys (Hu et al., 2020), and Spectral Analysis of Surface Waves (SASW) (Amin et al., 2022). Among these, ERT is gaining prominence as

an effective technique for subsurface characterisation (Samouelian et al., 2003). ERT necessitates less expertise, incurs lower operational costs, operates more quickly, and requires fewer manpower (Cosenza et al., 2006; Naseem et al., 2020).

However, the relationship between ERT and geotechnical parameters is highly site-specific, influenced by local mineralogy, pore fluid chemistry, and geological history. Previous studies have established correlations in various geological settlings, but no such comprehensive framework exists for the Lubok Antu region. This gap hinders the effective application of ERT for geotechnical engineering projects in this area.

This study fills a critical gap in the existing regional and global correlations between Electrical Resistivity Tomography (ERT) and geotechnical parameters like Standard Penetration Test (SPT) in the Lubok Antu region, which has unique geological characteristics such as melange structures and a clay-silt dominated matrix. While previous studies have explored ERT-SPT correlations in various regions, these efforts are often limited to specific soil types or geographical conditions, with little focus on areas with complex geological formations like Lubok Antu. By establishing robust ERT-SPT correlations tailored to this region’s specific conditions, this study advances the field by providing a new approach for geotechnical site characterisation in similarly challenging terrains. The unique integration of ERT and SPT data offers more accurate subsurface analysis, enhancing site assessment practices for both engineering and environmental applications.

Shear wave velocity (V_s) is crucial parameter for understanding soil and rock behavior under seismic loading, classifying seismic hazards at sites, designing earthquake-resistant structures, and ensuring the stability and safety of civil engineering projects (Abbas et al., 2024; Najar et al., 2022, 2025). It also aids in designing foundations that can withstand dynamic loads from sources like wind, waves, and earthquakes (Wang et al., 2018). Several authors reported that the combined parameters of V_s and electrical resistivity (ρ) facilitate the interpretation of soil types across various geotechnical sites (Goff et al., 2015; Lee and Yoon, 2015). The application of ERT in tropical and weathered terrains presents unique challenges (Dick et al., 2025; Sunny et al., 2024). For example, the resolution depth limits and spatial interpolation accuracy can vary significantly depending on soil types and local geological conditions. In tropical regions, where soils often exhibit high heterogeneity, factors such as moisture content, mineral composition, and weathering influence the interpretation of resistivity data (Zhao et al., 2021). Recent studies (Ijaz et al., 2025; Ijaz et al., 2023a; Ijaz et al., 2023b) have further explored these challenges, suggesting that a more nuanced understanding of these variables is crucial for improving ERT's reliability in such environments. Akin et al. (2011) developed an empirical relationship between V_s and Standard Penetration Test (SPT) - N values to propose a site-specific formula for obtaining V_s profiles for all layers in the Erbaa region of Turkey. The SPT - N involves driving a standardised sampler into the ground and recording penetration depths, providing critical insights into soil and geological conditions (Anbazhagan et al., 2012). Data collected at

multiple depths allow for depth profiles revealing variations in V_s. Alel et al., (2018) used ρ values and hybrid Artificial Neural Network-Particle Swarm Optimisation (ANN-PSO) method to estimate SPT - N. Tarmizi et al., (2016) integrated SPT - N values with Mackintosh probe results (M-values) and ρ values to explore soil properties at Universiti Sains Malaysia. Chang et al., (2011) examined the computation sensitivity and prediction accuracy of several SPT - N based methods using liquefaction and non-liquefaction incidents from the 1999 Chi-Chi Earthquake in Taiwan. Seed et al., (1985) correlated SPT - N values with field observations of soil liquefaction in Japan and China. Bajaj and Anbazhagan (2019) conducted seismic site characterisation and classification for the Indo-Gangetic Basin (IGB) considering V_s at various depths.

ERT has also been employed to investigate soil moisture dynamics in various regions, including Mediterranean southern France (Alamry et al., 2017), the central part of the Netherlands (de Jong et al., 2020), forest sites in Bavaria, Germany (Fäth et al., 2022), the BIONICS embankment in northeast England, and the Victorian embankment in central England (Gunn et al., 2015). Thus, ERT presents a viable alternative or supplementary approach (Akingboye, 2025) for acquiring data on soil moisture dynamics and its spatial distribution (Ahmad et al., 2024; Samouelian et al., 2005). This study aims to develop a unified correlation framework between ERT-derived resistivity and key geotechnical parameters (SPT-N, V_s, □) specifically for Lubok Antu region. The objectives are to (i) establish quantitative relationships between ρ and

SPT - N, V_s and □; (ii) analyse the practical mechanisms governing these correlations; and (iii) evaluate the practical applicability of these relationships for preliminary assessment.

2. Study Area and its Geotechnical and Geological Features

Lubok Antu is a district in Sarawak, Malaysia, situated on Borneo Island, near the border with Kalimantan, Indonesia shown in Fig. 1(a) as the blue region. The study area is located between longitudes 111°30'10.456"E and 112°14'13.712"E, and latitudes 0°59'4.676"N and 1°29'9.328"N, covering a total area of 2,395.54 km². The soils in Lubok Antu primarily originate from sedimentary rock formations, predominantly shale and coarse-grained sandstones, exhibiting considerable variability in texture, structure, and chemical composition (Wasli et al., 2011). According to the Sarawak soil classification system, these soils are categorised under the Kapit family of the Skeletal Soil Group (Teng, 2003), which corresponds to the Udorthents in the USDA (United States Department of Agriculture) soil

c n of t

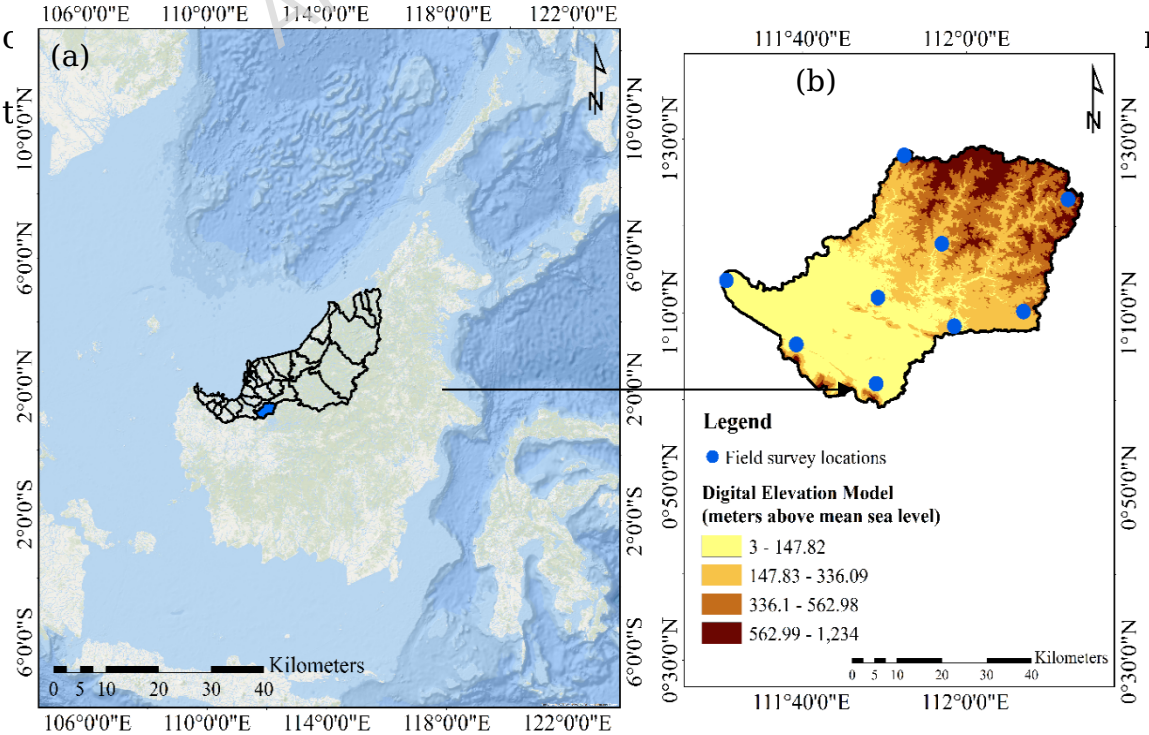

Fig. 1. (a) Geographical location of Sarawak, Malaysia, with the study area, Lubok Antu, highlighted as a blue polygon. (b) Field survey locations, represented by blue dots, overlaid on the Shuttle Radar Topography Mission (SRTM) digital elevation model, indicating sites where ERT and SPT data were collected.

The Lubok Antu region, located along the Lupar Line in West Sarawak, Malaysia, is known for its notable hydrogeological and geotechnical features, making it a key area for studies related to geophysical exploration (Haile, 1968; Hall & Breitfeld, 2017; Hutchison, 2005). The region's melange structure, which includes a sheared pelitic matrix interspersed with sandstone, mudstone, and chert clasts, shows considerable variation in permeability (Mathew et al., 2016; Tan 1982; Tjia, 1998). Extensive weathering, marked by reduced calcium and sodium levels, has contributed to a high fine content within the soil, which increases the likelihood of particle movement (Mathew et al., 2016; Zhao et al., 2021). Additionally, tectonic activity has created fractures and steeply inclined strata, which promote localised seepage and water flow (Madon, 2005; Shah et al., 2018; Zhao et al., 2021). These combined factors make the Lubok Antu region a significant area for examining soil properties. The location of the study area is shown in Fig. 1(b).

SPTs were conducted to a depth of 30 meters, with undisturbed samples collected at specified intervals to assess the soil’s engineering properties.

In geotechnical investigations, the SPT blow count, NSPT (number of blows required for 30 cm penetration of the sampler), serves as an indicator of soil shear strength and stiffness (Goncalves et al., 2021). Laboratory testing of the soil samples was carried out in accordance with ASTM (American Society for Testing and Materials) standards to ensure the accuracy and reliability of the results.

2.1 Geotechnical Dataset: Standard Penetration Tests (SPT)

The SPT is a widely used method for subsurface soil investigation, with SPT - N values commonly applied in geotechnical design to determine soil properties like strength and density (Hegde and Anand, 2022; Hossain et al., 2022). While effective, the requirement for a pre-drilled borehole makes SPT time-consuming and expensive.

Geophysical methods, particularly ERT, offer faster, cost-effective alternatives for subsurface characterisation due to their non-invasiveness and minimal operational complexity (Dezert et al., 2019; Oh and Sun, 2008). ERT has become popular for its low expertise requirements and efficiency in obtaining subsurface data (Drahor et al., 2006; Ismail and Yaacob, 2018; Lech et al., 2020). Borehole sample data is provided in Fig. 2.

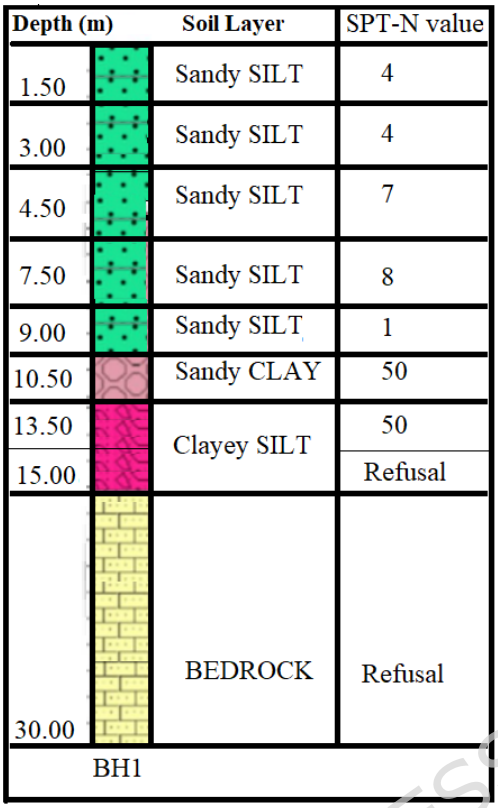

Fig. 2. Soil profile according to SPT

Correlations between SPT - N values and soil resistivity have been explored in numerous studies, revealing both linear (Hatta and Osman, 2015; Liu et al., 2008) and nonlinear relationships (Braga et al., 1999). Similarly, V_s, a critical parameter in geotechnical and seismic analysis, has been shown to exhibit nonlinear correlations with resistivity (Meju et al., 2003; Srivastava et al., 2010). However, research linking these parameters remains limited. Additionally, studies have explored the relationship between resistivity and other soil properties, such as hydraulic conductivity and density, further enhancing the understanding of subsurface conditions (Cosenza et al., 2006; Duan et al., 2019).

Globally, correlations between resistivity, SPT - N, and V_s are still under-researched, particularly at regional scales, necessitating localised

investigations (Akin et al., 2011; Rezaei et al., 2018). For example, in the Lubok Antu region, establishing these correlations will simplify geotechnical parameter determination through resistivity measurements, following the trends observed in São Paulo, Brazil, and Golestan Province, Iran (Braga et al., 1999; Rezaei et al., 2018).

V_s is a key parameter for evaluating soil stiffness and seismic properties. Although wave propagation tests are commonly used to determine V_s profiles, they are often expensive. Therefore, reliable correlations between V_s and SPT - N can help estimate V_s in regions lacking direct data (Kirar et al., 2016). Literature provides numerous equations that describe the correlation between SPT - N and V_s. These correlations vary depending on factors such as material type (sand, silt, clay), depth, fines content, corrected penetration resistance $(N1)_{60}$, and geological age. Table 2 summarizes the previously published empirical formulas that specifically relate uncorrected SPT - N values to V_s.

Table 1. Existing correlations between uncorrected SPT - N values and V_s.

Author(s)	All soils (m/s)	Sand (m/s)	Silt (m/s)	Clay (m/s)
Ohba and Toriuma (1970)	$V_s = 84\ N^{0.31}$			
Ohta et al., (1972)		$V_s = 87.2\ N^{0.3}$		
Imai et al., (1975)	$V_s = 89.9\ N^{0.34}$			
Imai (1977)	$V_s = 91\ N^{0.337}$	$V_s = 80.6\ N^{0.3}$		$V_s = 80.2\ N^{0.29}$

Seed and Idriss (1981)	$V_s = 61.4\ N^{0.5}$			
Okamoto et al., (1989)		$V_s = 125\ N^{0.3}$		
Lee (1990)		$V_s = 57.4\ N^{0.4}$	$V_s = 105.64\ N$	$V_s = 114.43\ N^{0.}$
Dikmen (2009)	$V_s = 58\ N^{0.39}$	$V_s = 73\ N^{0.33}$	$V_s = 60\ N^{0.36}$	$V_s = 44\ N^{0.48}$
Uma Maheswari et al., (2010)	$V_s = 95.64\ N^{0.3}$	$V_s = 100.53\ N$		$V_s = 89.3\ N^{0.358}$
Gautam (2017)	$V_s = 115.8\ N^{0.2}$	$V_s = 78.7\ N^{0.3}$	$V_s = 102.4\ N^{0.}$	

The empirical equations for estimating shear wave velocity (V_s) were selected based on their widespread use and validation in geotechnical and seismic engineering literature. Specifically, equations such as thoese proposed by Imai and Tonouchi (1982) and Ohta and Goto (1977) were employed, as these have been proven to provide reliable estimates for V_s and SPT-N values. These equations are widely accepted in areas with similar geological conditions, such as tropical and sedimentary soils, and have been used successfully in precious studies (e.g., Bajaj and Anbazhangan, 2019). These empirical correlations offer a practical method for estimating V_s in the absence of direct shear wave velocity measurements, making them suitable for large-scale site investigations.

Uncorrected SPT-N values were preferred in this study due to their direct availability from standard geotechnical testing and their proven reliability for estimating soil strength and stiffness. While corrected SPT-N values (e.g., N60) are commonly used to account for factors such as overburden pressure, uncorrected SPT-N values are sufficient for this study based on

their widespread use in previous studies (e.g., Akin et al., 2011; Bajaj and Anbazhagan, 2019). Furthermore, in regions like Lubok Antu, uncorrected SPT-N values provide a more practical and cost-effective method for preliminary site investigations. These values have shown a strong correlation with V_s and other geotechnical parameters, making them appropriate for this unique geological conditions of the region.

2.2 Geophysical Dataset: Electrical Resistivity Tomography (ERT)

Electrical resistivity is a critical parameter in soil characterisation, influencing how well soil conducts electricity. Factors like porosity, mineral composition, moisture content, sensitivity, and plasticity index can affect resistivity (Archie, 1942; Chu et al., 2018; Devi et al., 2017). ERT has been widely used to identify soft clays and assess soil consolidation (Saneiyan et al., 2018; Snapp et al., 2017). Quick clay, identified by a sensitivity greater than 30 and remolded undrained shear strength less than 0.5 kPa, is effectively delineated using ERT (Malehmir et al., 2013; Solberg et al., 2016). In contrast, SPT require boreholes, adding to cost and time constraints (Fatehnia et al., 2015; Hatta and Osman, 2015; Hussien and Karray, 2015; Sudha et al., 2009). Geophysical methods like ERT, which are non-invasive, faster, and more cost-effective, are gaining popularity in geotechnical research (Islam et al., 2020; Ismail and Yaacob, 2018; Lech et al., 2020). Among these methods, ERT is particularly effective due to its operational simplicity and lower costs (Hegde and Anand, 2022).

Numerous studies have explored correlations between soil resistivity, SPT - N values, and shear wave velocity (V_s). Imai and Tonouchi (1982) developed the relationship between V_s and SPT - N in Japan, while subsequent research extended these correlations to other regions using various geophysical methods (Wair et al., 2012). In Malaysia, Hatta and Osman (2015) reported a linear relationship between SPT - N and sandy soil resistivity using the Wenner array. Rezaei et al., (2018) established similar correlations in Iran, and Sudha et al., (2009) observed a linear relationship between SPT - N and resistivity in India. The current study seeks to establish specific correlations for soil in Lubok Antu, Sarawak, where such relationships remain underexplored.

3. Methodology

This study explores the correlations between the soil electrical resistivity and index geotechnical parameters focusing on Lubok Antu region of Sarawak, Malaysia. The study has been carried out in different phases to achieve the aim of this paper. The methodology is designed to simulate correlations under controlled conditions to assess the soil resistivity and evaluate the geotechnical parameters. The flowchart of this study is shown in Fig. 3.

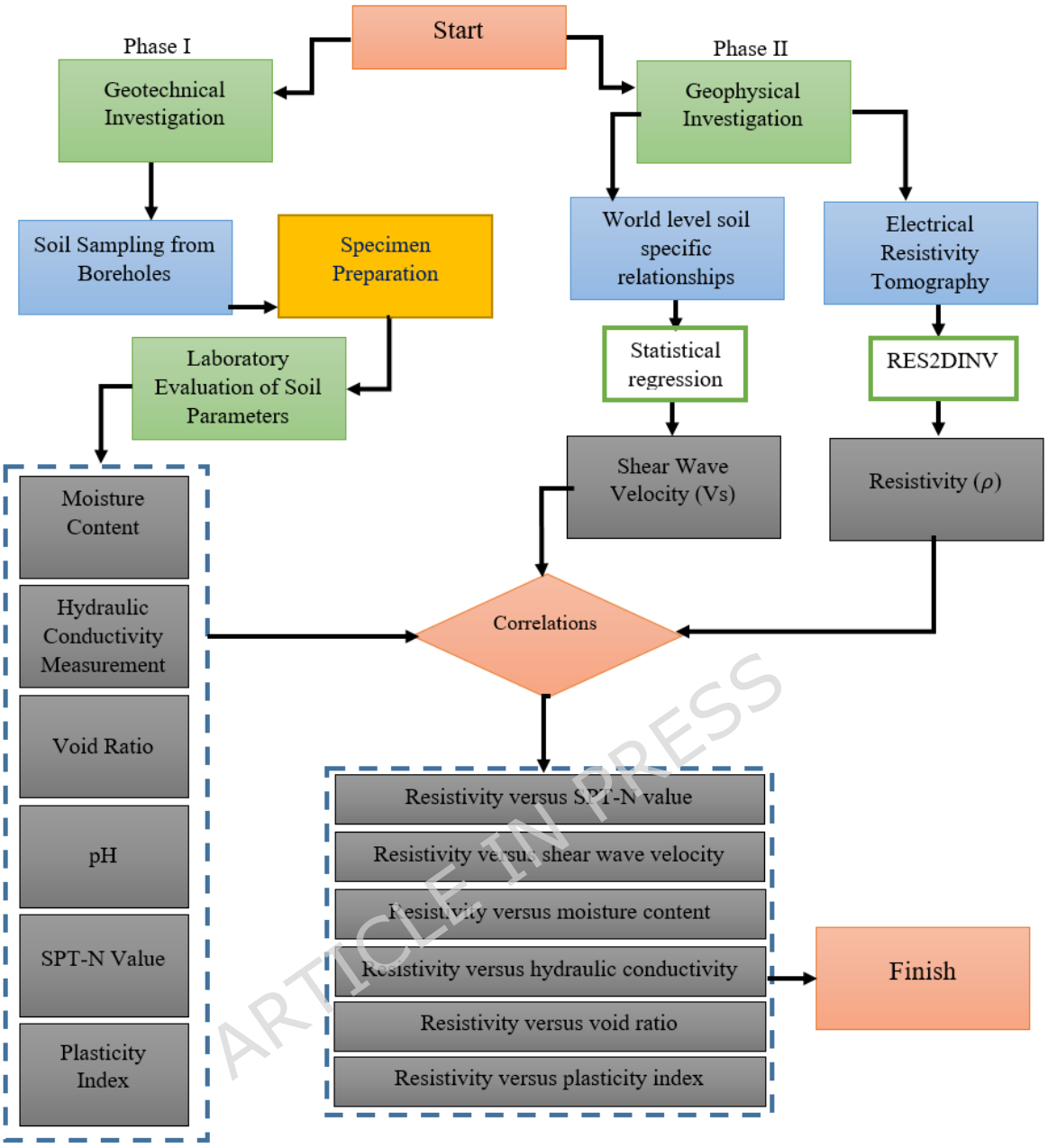

Fig. 3. Flow of this study

3.1 Geophysical investigation – Electrical Resistivity Tomography (ERT)

A total of nine locations in Lubok Antu were identified for SPT and ERT, with data collected from these specific sites. Fig. 4(a) and Fig. 4(b) display images of the on-site field investigations for SPT and ERT, respectively.

Fig. 4. (a) SPT investigation, and (b) experimental setup for the ERT experiment conducted in the field

The ERT procedure involves applying Ohm's law using a minimum of four electrodes, as depicted in Fig. 5. For this study, the Wenner-Schlumberger electrode array was employed, utilizing 20 stainless-steel electrodes. These electrodes, each 0.6 meters in length and 0.012 meters in diameter, were spaced 5 meters apart and inserted to depths of up to 0.45 meters. After each measurement, the electrodes were repositioned.

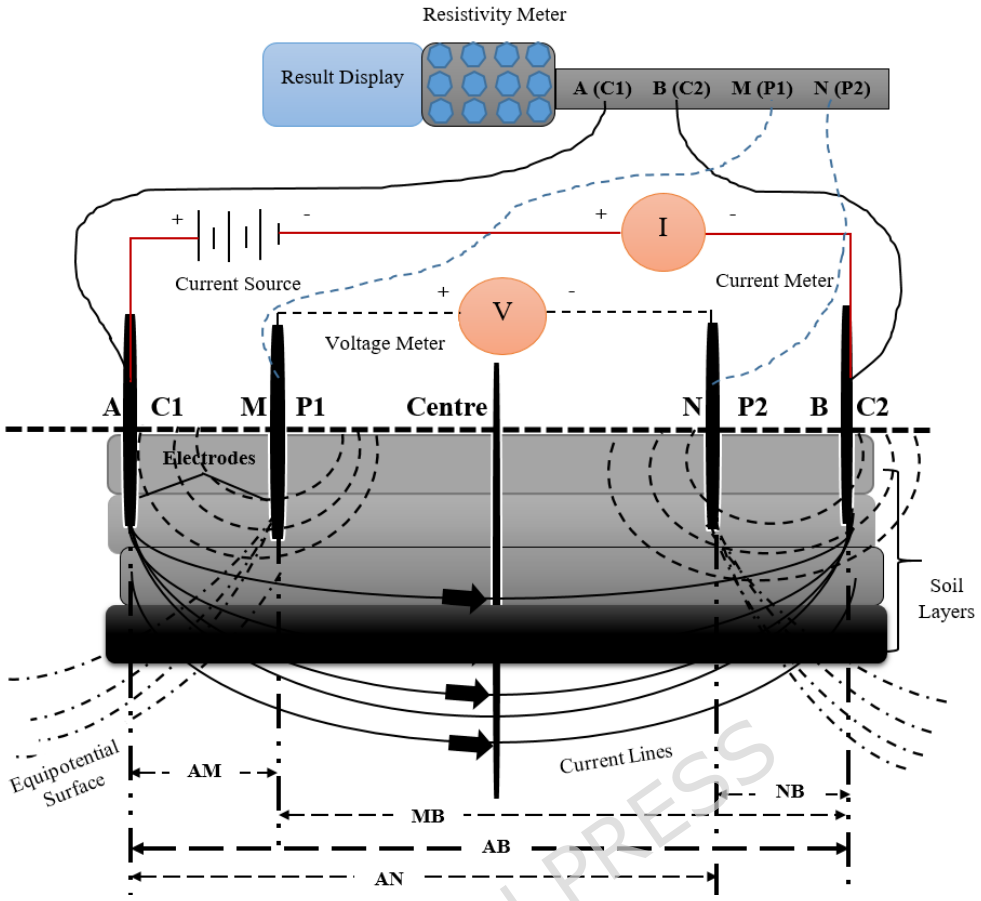

Fig. 5. Schematic Illustration of the ERT

To obtain the measurements, the outer electrodes (C1 and C2) were connected to a direct current source, while the inner electrodes (P1 and P2) recorded the corresponding potential drop. The Wenner-Schlumberger array, known for its symmetric and collinear arrangement, was used to determine the soil resistivity. In this configuration, the current electrodes are spaced farther apart than the potential electrodes, enabling the measurement of soil resistivity beneath the central electrode, typically equivalent to $\frac{AB}{3}$. This method is favoured for its efficiency and reduced contact issues, as only the current electrodes need to be repositioned after each reading. In this study, the Geomative resistivity meter (GD-10

Supreme V2.5.1T28) was used to conduct nine ERTs at the same locations as the SPTs, with both tests reaching a depth of 30 meters. The electrodes were spaced 5 meters apart, and measurements were taken sequentially with a roll-along strategy, moving the electrodes by 5 meters after each reading. A total of 3 readings were taken at each station to ensure accuracy. The maximum electrode separation used was 15 meters to ensure adequate depth resolution. 5% error threshold was maintained in resistivity measurements and excluded data points that exceeded this error margin. Electrodes were cleaned before each use, and contact resistance was monitored continuously. If any readings indicated high contact resistance, they were discarded.

$$\rho = \frac{\pi \times S^2}{a} \times \frac{\Delta V}{I} = K\frac{\Delta V}{I} \quad (1)$$

where, ρ represents the apparent resistivity, ΔV is the measured voltage difference, I is applied current, and K denotes the geometric constant, which is defined as:

$$K = \frac{\pi \times S^2}{a} \quad (2)$$

S is half the distance between the current electrodes A and B $\left(S = \frac{AB}{2}\right)$, and a represents the distance between M and N.

Previous studies have demonstrated that soil resistivity is influenced by factors such as mineralogy, temperature, and moisture content (Hegde and Anand, 2022). However, this study took steps to minimize the impact of these variables. To mitigate the effects of moisture and temperature, ERT measurements were conducted during the dry season. Additionally,

soil moisture and temperature levels at the different study locations showed minimal variation, with differences of less than 3% and 1%, respectively. Chemical analyses were performed to assess the pH, sulfate content, and chloride content at various locations. The pH values ranged from 4.36 to 6.78, while sulfate and chloride concentrations varied from 0.02% to 0.07% and 0.01% to 0.04%, respectively. Organic content was found to range between 0.34% and 2.50%. According to Dafalla and AlFouzan (2012), the chemical properties of soil have a less significant effect on resistivity compared to particle size distribution (PSD), though it should be noted that sulfate and chloride content can lower soil resistivity.

ERT measurements were taken at different locations within the Lubok Antu region, in alignment with the locations of the SPT. To extract resistivity values from the inversion cells at corresponding borehole depths, this study applied the Res2Dinv inversion software (Blanchy et al., 2020). The inverted resistivity sections were carefully analysed to account for depth resolution limitations, as resistivity measurements at greater depths tend to be more smoothed due to the inherent smoothing effect of the inversion process. The extracted resistivity values were verified for consistency across the depth range, and erroneous or outlier values due to local geological effects were excluded from the dataset. Additionally, the depth precision of the resistivity measurements was determined based on the electrode spacing and the inversion cell size, ensuring that the resistivity values correspond to the appropriate subsurface zones. The processed data were then interpolated in a Geographic Information System (GIS) environment using Spatial Analyst tools to create resistivity

contour maps at various depths, including 1.5 m, 4.5 m, 7.5 m, 10.5 m, 12 m, 13.5 m, 15 m, and 25 m. These datasets were harnessed to establish the relationship of ρ with V_s, $SPT - N$ values, and w.

A significant challenge in this study involves extracting depth-specific resistivity values from the ERT data. The inversion process inherently involves smoothing, which can reduce the depth resolution at greater depths. Resistivity values obtained from ERT are averaged over larger regions (often 1-2 meters in depth), and these values may not correspond exactly to the localised measurements taken at boreholes. To mitigate this issue, we focused on shallow depths (up to 10 meters), where the depth resolution of the inversion process is more precise. Additionally, we applied inversion model sensitivity analysis to assess the impact of smoothed resistivity values on local geotechnical behaviour, noting that the observed correlations remain robust despite these resolution limitations. The inversion resolution was further discussed, particularly how the depth of investigation impacts the precision of subsurface resistivity profiles.

3.2. Geotechnical Investigation - Laboratory Evaluation

Geotechnical investigations are used to assess the properties of the soil at specific locations. The standard penetration test (SPT) involves driving a standard sampler into the ground and recording the number of blows required to penetrate the soil a specific depth. This test helps in assessing soil stiffness, cohesion, and friction angle, which are essential for geotechnical engineering and foundation design. Additionally, the grain

size distribution analysis of soil samples provides information about the composition of the soil, including the percentage of sand, silt, and clay, which can influence the soil's permeability and engineering properties. Borehole data were crucial for calibrating the ERT results, allowing for a more accurate interpretation of the subsurface conditions.

Borehole data, obtained by drilling holes into the ground and recording subsurface information, are crucial for validating and improving the accuracy of ERT results. By comparing the resistivity values from ERT with the actual soil properties measured in boreholes, a correlation can be established. This correlation aids in converting electrical resistivity data into meaningful geotechnical and geological information, enhancing the reliability of the findings. In conclusion, the field investigations carried out in this study integrated geoelectrical (ERT) and geotechnical (SPT, grain size analysis) techniques to comprehensively understand the subsurface conditions. The utilisation of borehole data for calibration and correlation ensured the accuracy of the obtained results, enabling a more robust assessment of the geological and geotechnical properties of the study area.

3.2.1 Specimen Preparation

Soil samples were obtained during the standard penetration tests (SPT) to ensure they remained undisturbed, as shown in Fig. 6. A thin-walled sampler was driven into the soil at a steady rate, with minimal vibration, to preserve the natural structure and minimize disruption from shear forces. After collection, the samples were carefully wrapped in plastic and sealed in airtight containers to maintain moisture and protect them from

environmental exposure. The integrity of the samples was checked for signs of stratification, voids, or compression that could suggest disturbance. Following this, the samples were placed in a chamber for various laboratory tests, maintaining their original in-situ conditions. The moisture content (MC) was recorded at the start of the testing, and every effort was made to ensure that the soil structure was minimally disturbed during the sample handling and preparation. The more detailed explanation is provided in the doctoral thesis of first author of this paper.

Fig. 6. (a) Collected undisturbed soil sample (b) shaping of soil sample for suffusion testing (Najar et al., 2025)

The laboratory investigation of soil samples were carried out at Universiti Malaysia Sarawak (UNIMAS). The soil samples were collected depth wise during the SPT.

The laboratory investigations which were carried out are listed below:

i. pH
ii. Moisture content
iii. Bulk and dry density
iv. Specific gravity

v. Particle size distribution

vi. Atterberg limit

vii. Unconsolidated undrained triaxial test

viii. Hydraulic conductivity

All the geotechnical parameters have been determined in laboratory, the methodology is explained in Table 2.

Table 2. Laboratory testing methods

S.no.	Test	Equipment/Test Standard	Procedure
1	pH	Electrometric pH meter, Glass electrode, Saturated calomel electrode (SCE)	Soil samples were collected from the study area, calibrated electrodes were used for pH measurement, and standard buffer solutions (pH 4, 7, 10) were used for calibration. The pH was determined by immersing the glass electrode in the soil-water paste and measuring the stabilised potential. The test is shown in Fig. 7(a)
2	Moisture content	Weighing balance, Oven (105°C ± 5°C), Moisture cans, Desiccators (BS EN ISO 17892-1 (2014))	Soil samples were dried in a temperature-controlled oven until constant mass was achieved. Moisture content is calculated based on the mass change using the formula $MC\ (\%) = \frac{(M2-M3)}{(M3-M1)} \times 100$, where M1, M2, and M3 represent initial, total, and final mass, respectively.
3	Bulk and dry density	Weighing balance, Suitable volume containers (BS EN ISO 17892-2 (2014))	Bulk and dry density are determined by measuring the mass of soil samples and their volume. Bulk density $\gamma bulk = \frac{M1}{V2-V1}$ and dry density $\gamma dry = \frac{M2-M1}{V2-V1}$, where M1, M2 are mass, and V1, V2 are volume measurements.
4	Specific gravity	Pycnometer, Weighing balance (BS EN ISO 17892-3 (2015))	Specific gravity was measured using a pycnometer, and calculated as $Gs = \frac{M2-M1}{(M2-M1)-(M4-M3)}$, where M1, M2, M3, and M4 are the mass measurements at different steps of the process. The test is shown in Fig. 7(b)
5	Particle size distribution	Set of calibrated sieves, Weighing balance (BS EN ISO 17892-4 (2016))	Particle size distribution was determined by sieving the soil through a set of sieves, from largest to smallest. The masses of the soil retained on each sieve were recorded to calculate the distribution. The test is shown in Fig. 7(c)
6	Atterberg limit	Casagrande apparatus, Cone penetrometer, Standardised plastic limit dish (BS EN ISO 17892-12 (2018))	The liquid limit (LL) and plastic limit (PL) were determined by the number of blows required to close a groove in a soil sample (LL) and by observing the moisture content at which the soil exhibits plastic behavior (PL). The plasticity index (PI) is calculated as $PI = LL = PL$. The test is shown in Fig. 7(d).
7	Unconsolidated undrained triaxial test	Triaxial testing apparatus, Load frame, Data acquisition system (BS EN ISO 17892-8 (2018))	The UU triaxial test was performed by applying axial load to a soil sample in a triaxial cell, while measuring pore pressure and

			recording stress-strain data. The unconfined compressive strength was determined at failure. The test is shown in Fig. 7(e)
8	Hydraulic conductivity	Permeameter, Weighing balance, Stopwatch (BS EN ISO 17892-11 (2019))	The soil samples were saturated in the permeameter and the time required for the water head to fall is recorded. The hydraulic conductivity (K) is calculated using $K = \frac{2.3 \times a \times L}{A \times t}\left(\log \frac{h1}{h2}\right)$, where a is the cross-sectional area of the tube, L is the length, A is the area, and t is time. The test is shown in Fig. 7(f).

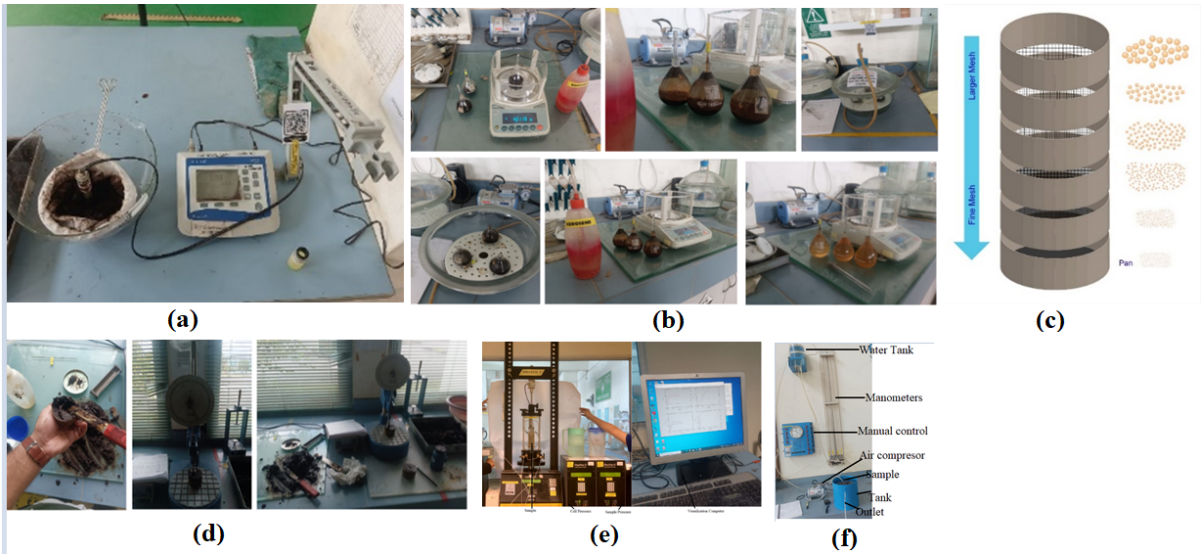

Fig. 7. Laboratory evaluation of geotechnical parameters (a) pH, (b) specific gravity, (c) particle size distribution, (d) Atterberg limits, (e) Triaxial test and (f) hydraulic conductivity

3.3 Regression and Correlation Analysis

As a fundamental statistical approach, regression analysis is extensively utilised to investigate associations in datasets and ascertain the individual impact of various variables. This principal goal of this study is to establish a relationship model incorporating two to four parameters via nonlinear regression, a process conducted using specialised analytical software. For this research, OriginPro is employed as the key platform for constructing a detailed statistical model and for testing the robustness and statistical significance of the identified variable correlations. OriginPro is a comprehensive graphing and data analysis application, renowned for its powerful tools tailored for scientific graphing and nonlinear curve fitting. Its capabilities include sophisticated data manipulation, the creation of publication-quality graphs, and the implementation of complex fitting algorithms. To rigorously quantify the error inherent in the nonlinear regression, the fitted quality and efficacy of model are assessed using the

coefficient of determination (r^2). Calculated from Equation 3, this statistic is a pivotal indicator of the model's capacity to account for the variance observed in the response data.

$$r^2 = 1 - \frac{\sum (y_i - \hat{y}_i)^2}{\sum (y_i - \overline{y}_i)^2} \quad (3)$$

Where,

y_i = tested data

$\hat{y}_i$ = prediction of least squares

$\overline{y}_i$ = mean of the statistical data

4. Results and Discussions

Fig. 8(a-i) presents the resistivity contour corresponding to the normalised error of ERT1, ERT2, ERT3, ERT4, ERT5, ERT6, ERT7, ERT8, and ERT9 Sites at Lubok Antu, illustrating resistivity variations down to a depth of 25 meters. The depth is expressed in terms of elevation, while resistivity is shown as the magnitude. This Fig. highlights the distribution of soil resistivity across the study area. Fig. 9(a-h) depicts change in resistivity with increasing depth up to 25 meters in the Lubok Antu region. The resistivity data were interpolated using the inverse distance weighted (IDW) technique in ArcGIS 10.8 ©, providing a smooth and continuous representation of values across the study area while minimizing overlap between zones. These measurements were taken near SPT locations, and an overall increase in resistivity with depth was observed. Notably, the Lubok Antu region has a higher percentage of clayey silt, which, due to the

negatively charged surfaces of clay particles, enhances soil conductivity and reduces resistivity. While moisture content can generally lower resistivity, the depth of the water table in this case suggests it had little influence on the observed values. Despite this, an interesting trend of increasing resistivity with depth was identified in the study area.

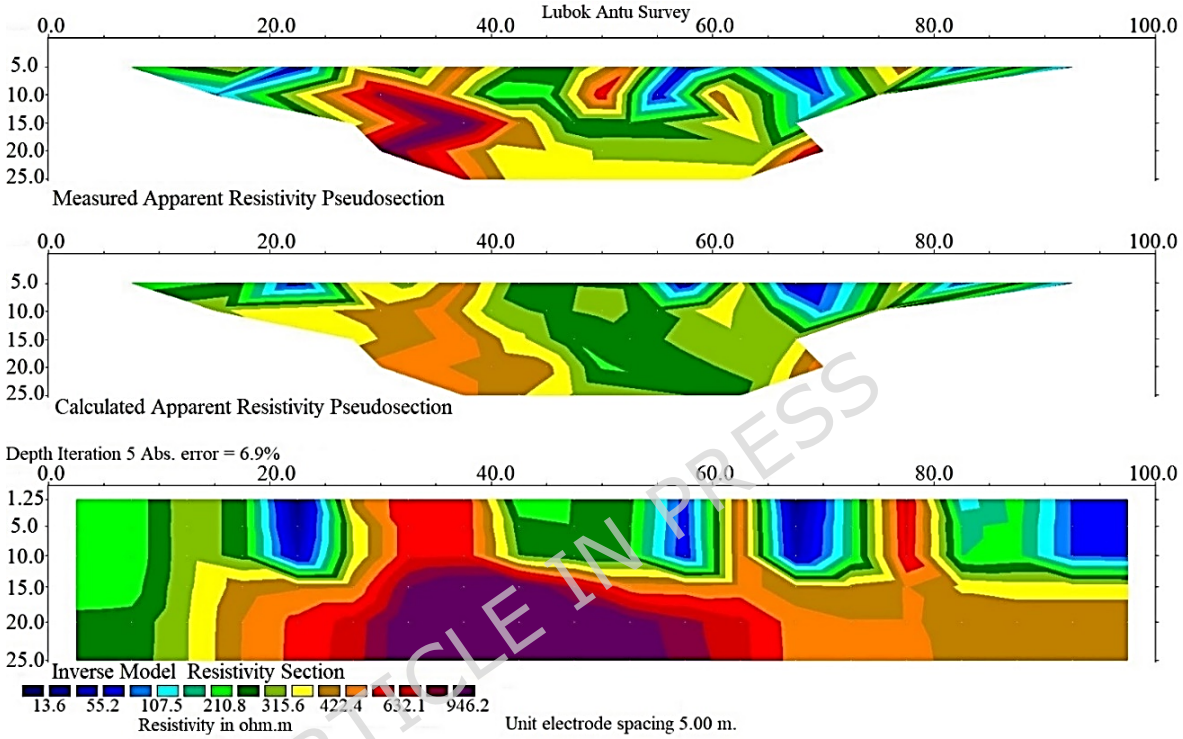

(a)

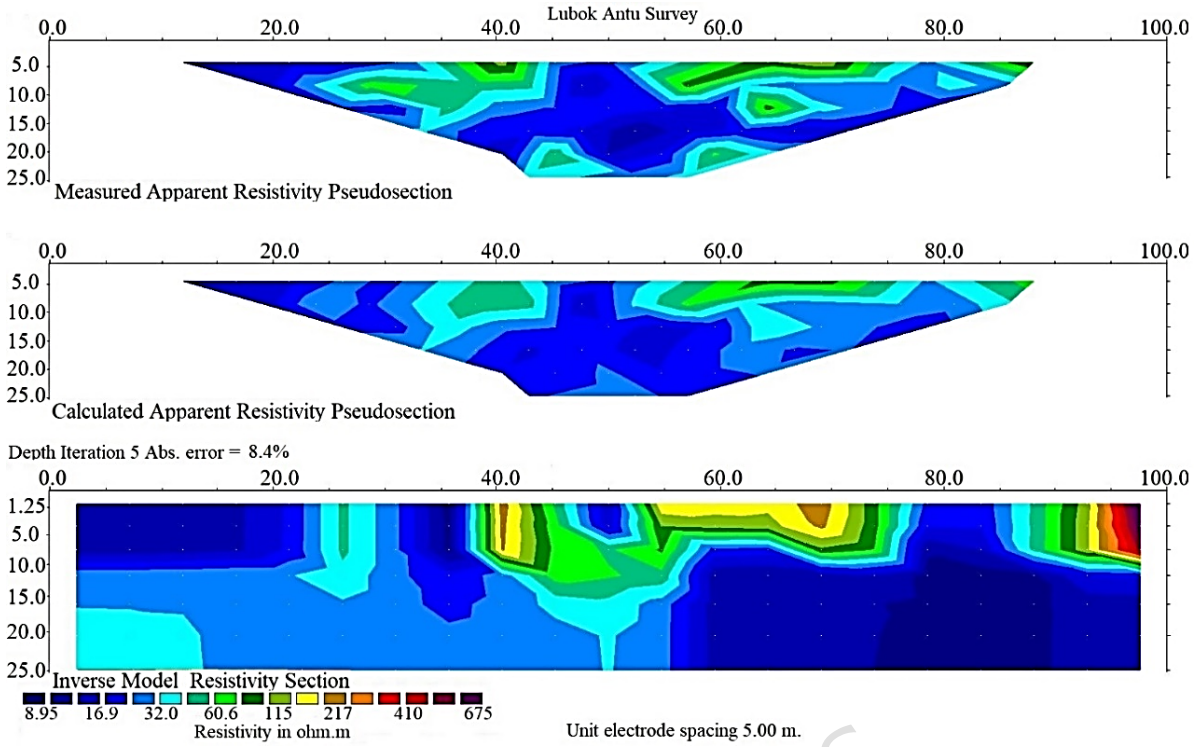

(b)

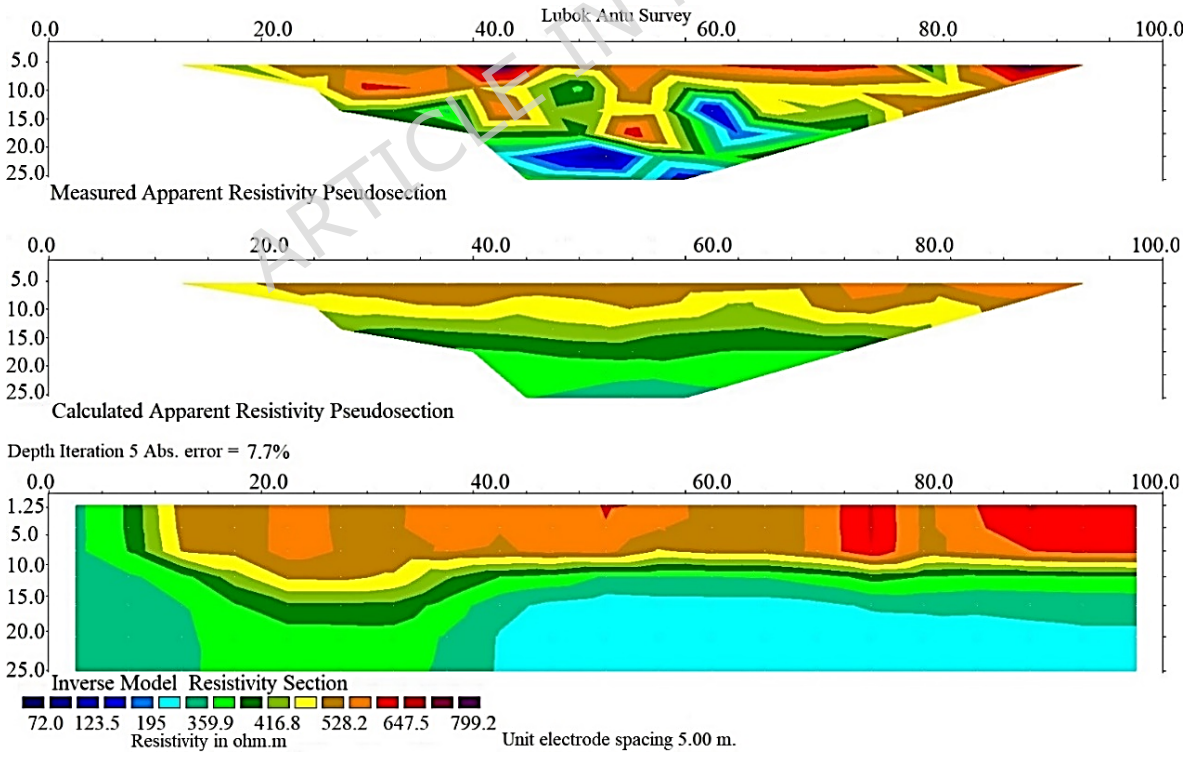

(c)

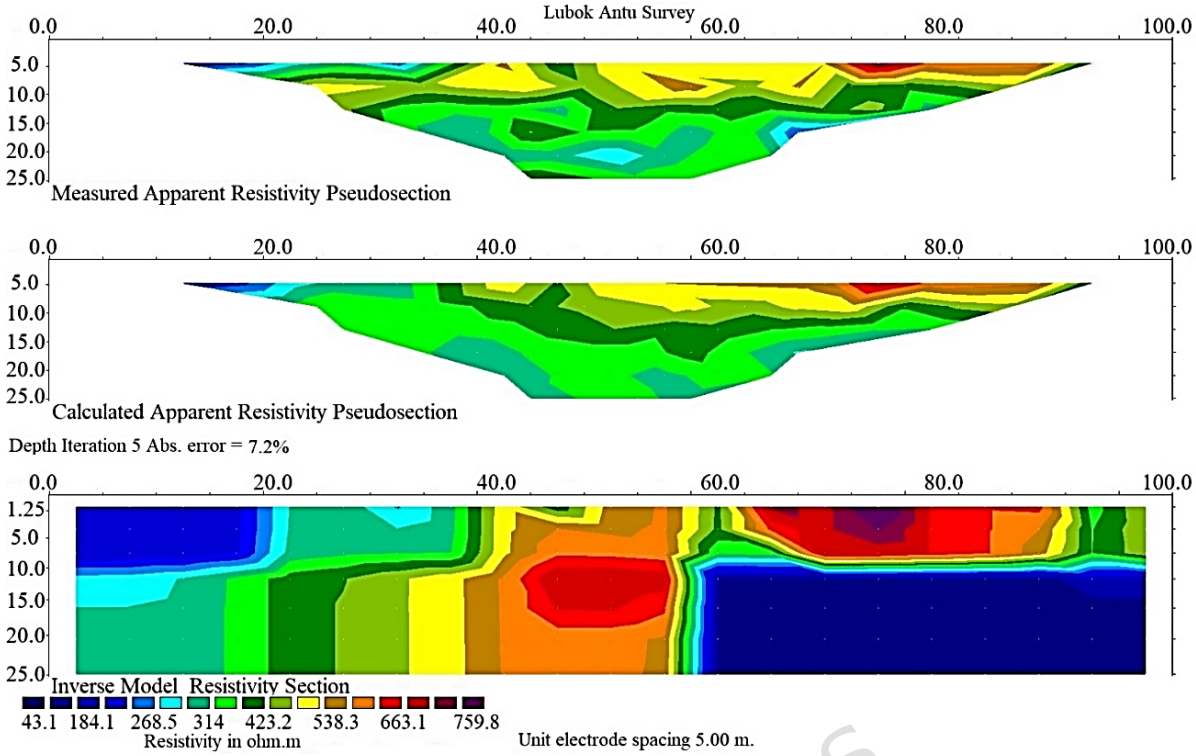

(d)

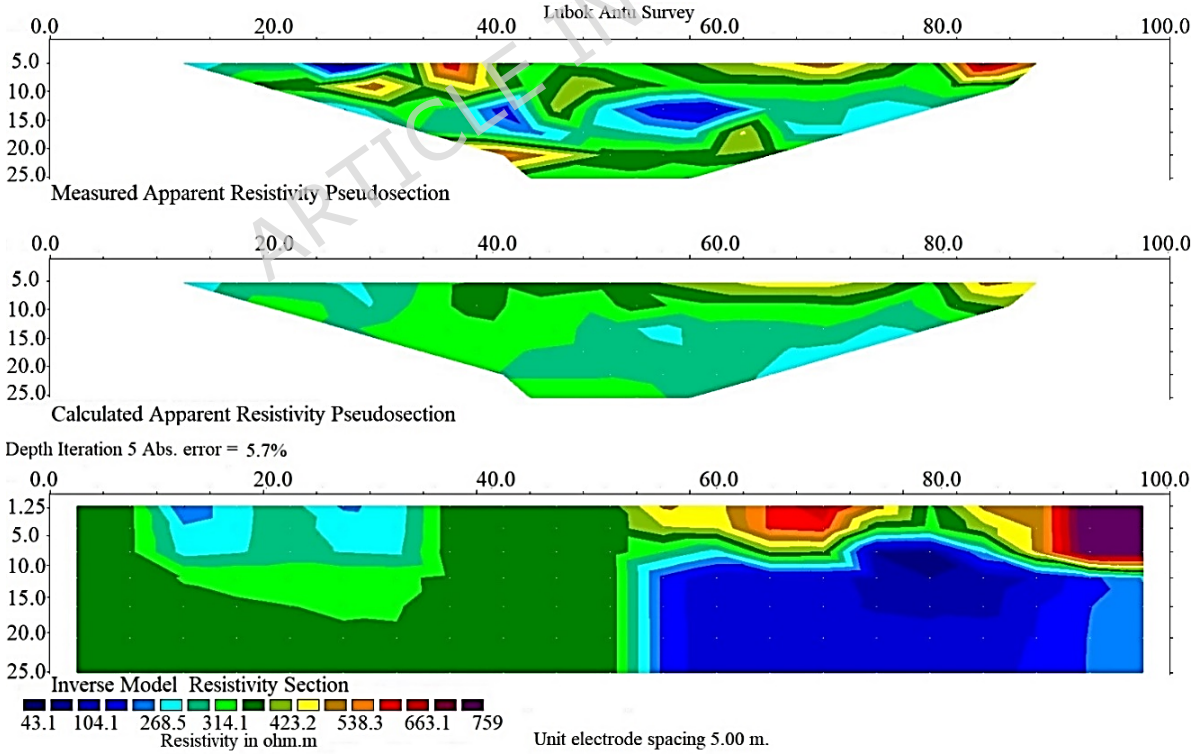

(e)

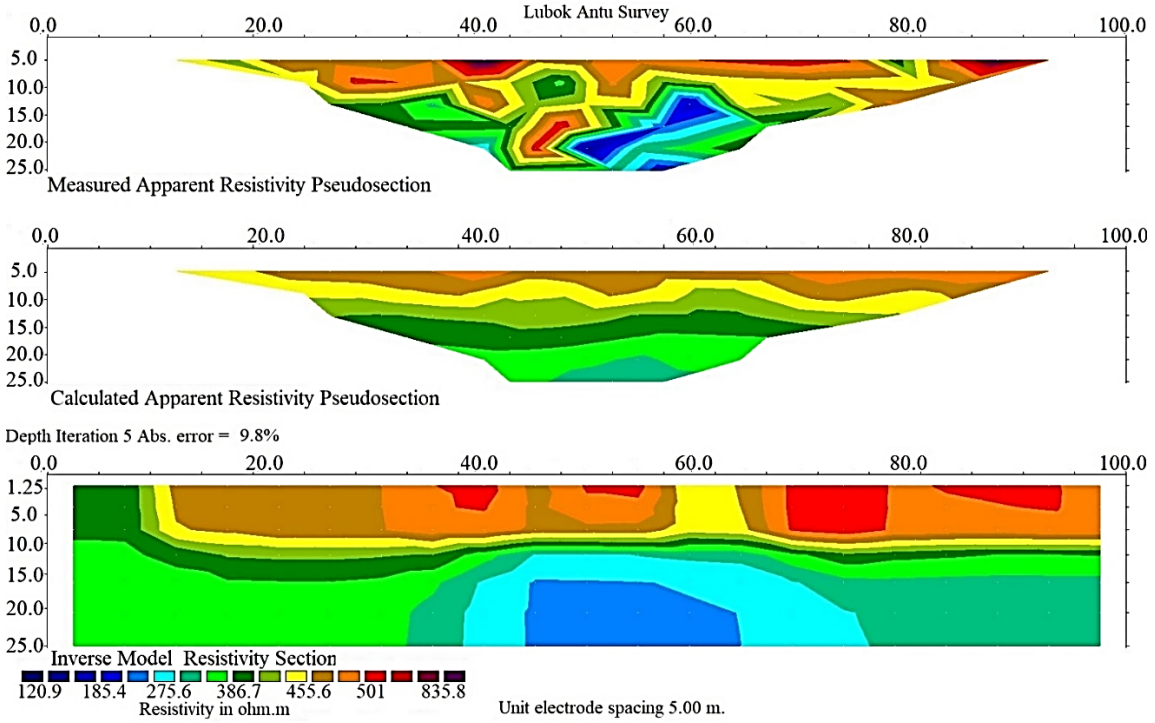

(f)

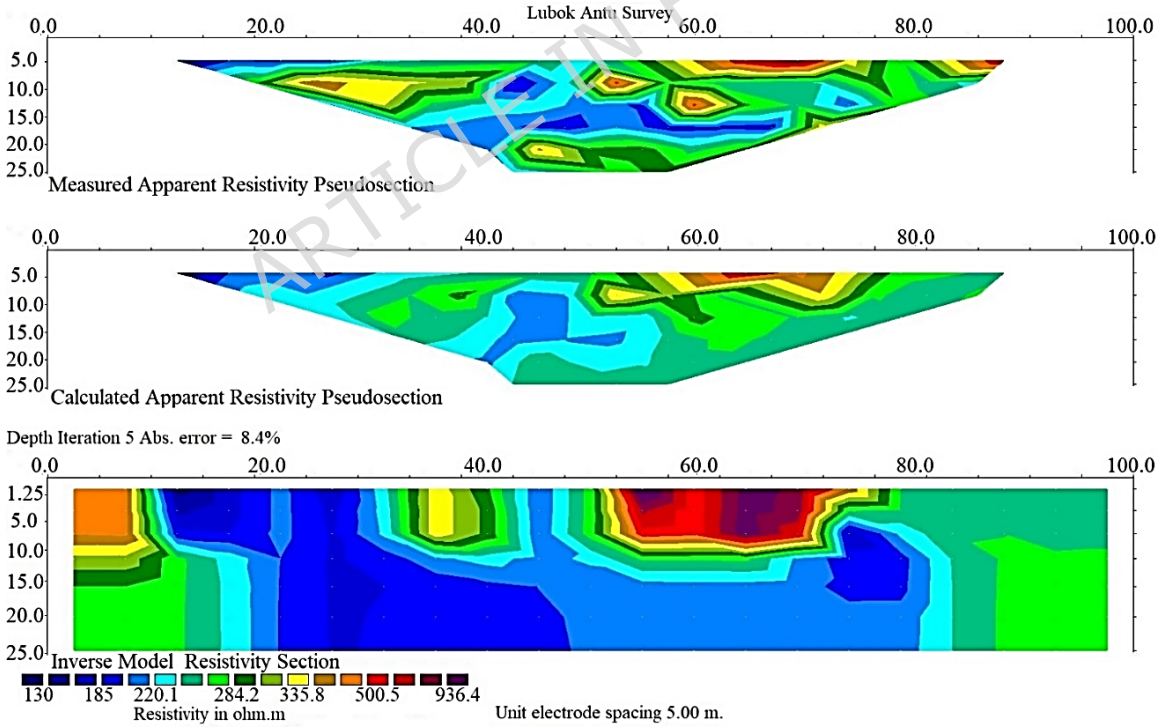

(g)

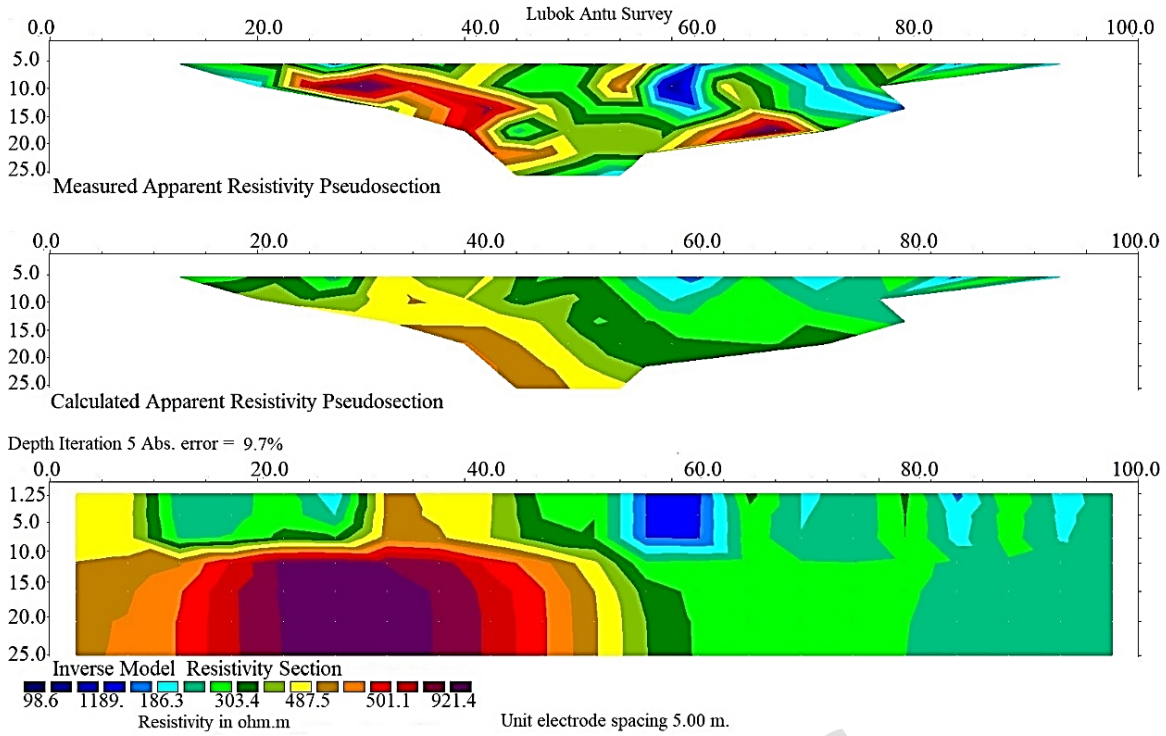

(h)

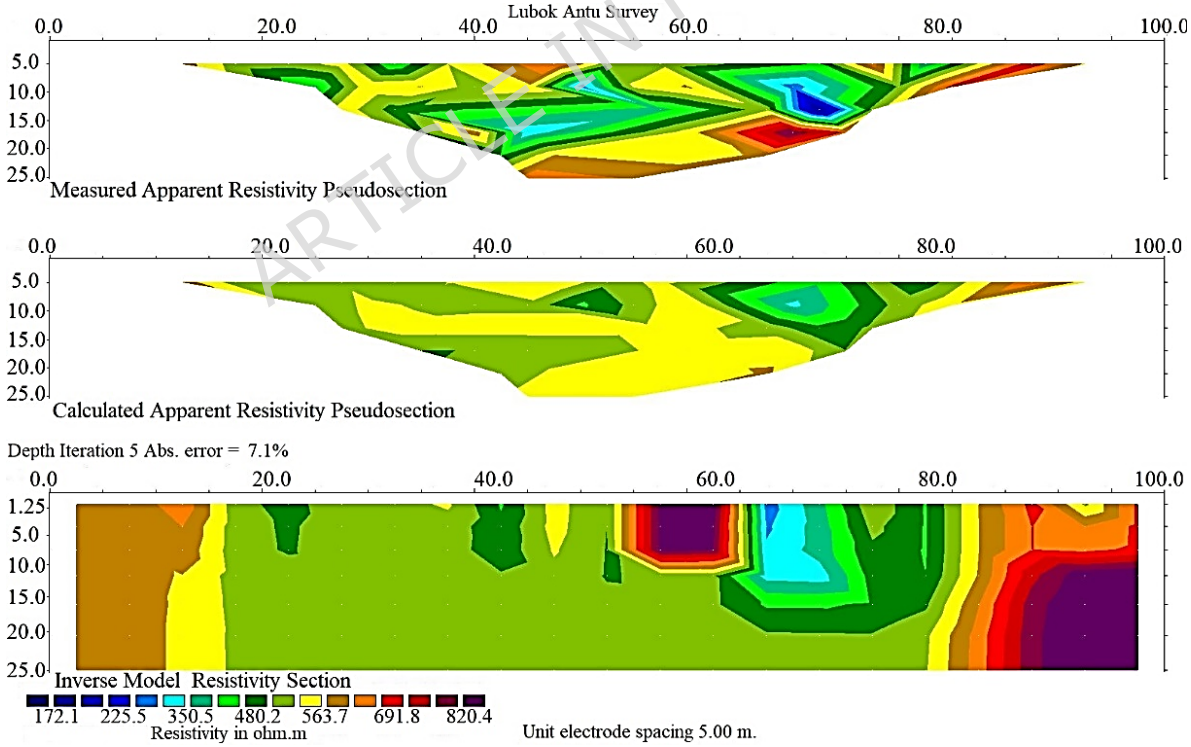

(i)

Fig. 8. (a-i) Sample of inversion of resistivity profile of ERT1, ERT2, ERT3, ERT4, ERT5, ERT6, ERT7, ERT8 and ERT9 sites at Lubok Antu

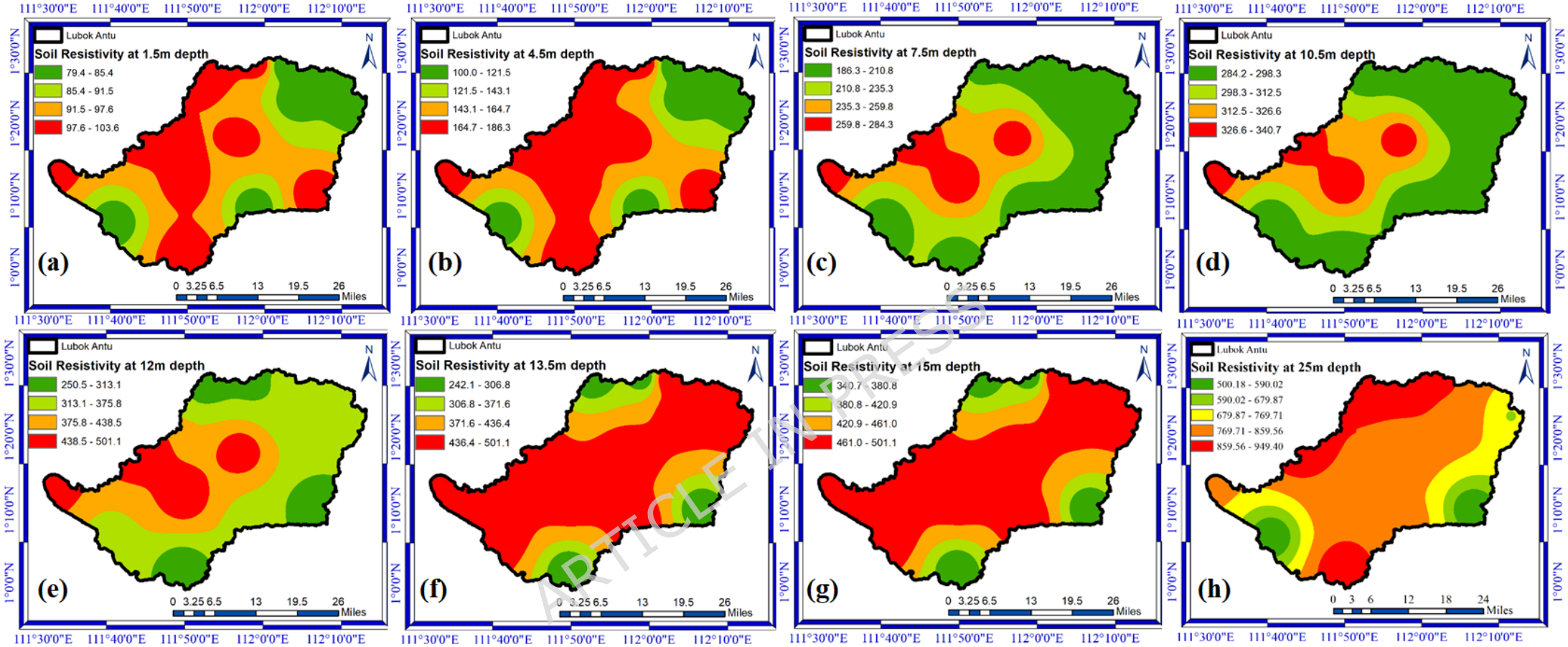

Fig. 9. Soil resistivity maps at various depths, highlighting resistivity changes across the Lubok Antu region with increasing depth

4.1 Determination of pH

The determination of soil pH in this study was conducted using the electrometric method, which is a widely accepted technique for assessing the acidity or alkalinity of soils. The investigation of soil pH at various depths revealed notable variations, indicating distinct acidity or alkalinity levels across different layers. Overall values of pH for all the layers of soil is in-between 4.3 to 6.8. The following observations were recorded; the topmost layer exhibited a nearly neutral pH of above 6, suggesting a mildly neutral environment. As the depth increased to, there was a noticeable shift towards increase in pH value, indicating a potential buffering effect in this layer. Within the transition zone of 4.5m to 7m, the soil demonstrated a value from 5.5 to 6.7. This shift may suggest variations in soil composition or organic content. In the deeper layers, between 9m to 15m, the soil displayed the values in between 6.7 to 5.8, indicating less acidic. These findings highlight the dynamic nature of soil pH with depth, signifying potential influences on nutrient availability, microbial activity, and overall soil health. The pH of soil layers of different boreholes corresponding to different layers is shown in Fig. **10**.

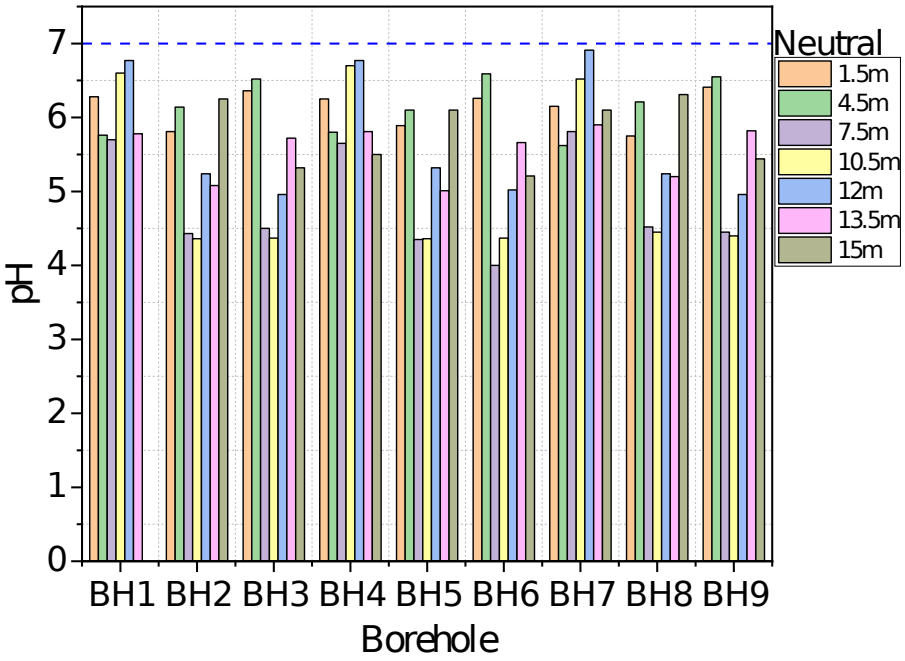

Fig. 10. pH of soil layers of different boreholes

4.2 Determination of Moisture Content

Moisture content is a measure of the amount of water present in a soil sample. It is an important parameter in soil testing, as it can affect many properties of the soil, such as its strength, compressibility, and density. In this study, moisture content was found in the range of 3% to 43%, from which it was found the soil between 10.5m to 13.5m depth has low moisture content. The results of moisture content are shown in Fig. 11.

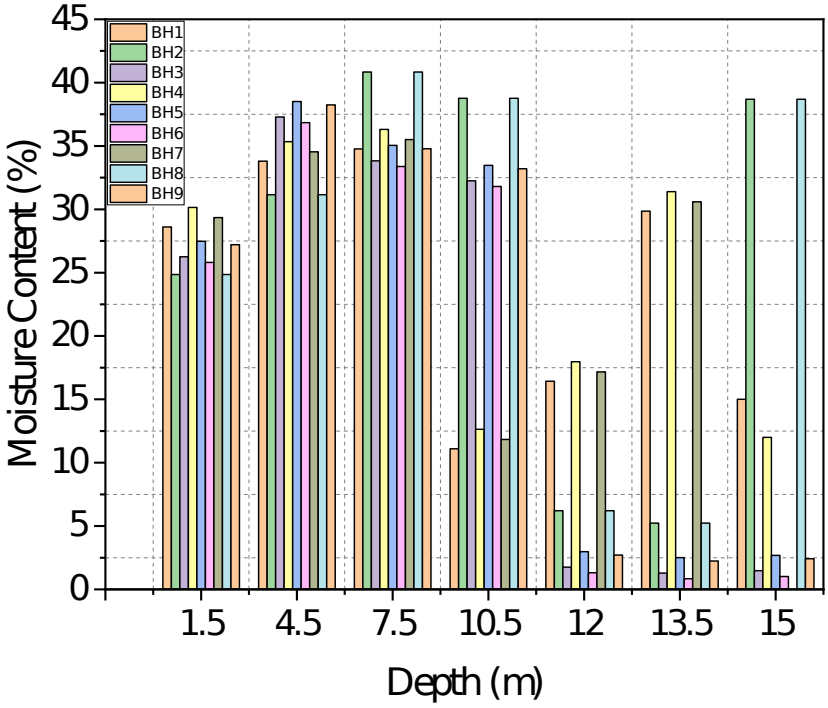

Fig. 11. Moisture content of different soil layers

4.3 Determination of Bulk and Dry Densities

After moisture was removed, the dry density of soil which is the mass of solids per unit volume was determined to be 1.46Mg/m^3. Conversely, the bulk density, which represents the total mass of soil (solids and pores combined) per unit volume, was found to be 1.83Mg/m^3. The relationship between bulk density and dry density sheds light on the porosity of the soil depicted in Fig. 12. A higher porosity, which implies that the soil has more pore space, is indicated by a lower bulk density. On the other hand, increased bulk density results in decreased pore space and increased soil compaction. Understanding water retention, nutrient availability, and general soil health depend heavily on these findings. To further highlight the state of the soil, values can be compared to standard benchmarks or previous measurements. Variations from predicted values could be a sign

of compaction problems in the soil, or other problems affecting the structure of the soil.

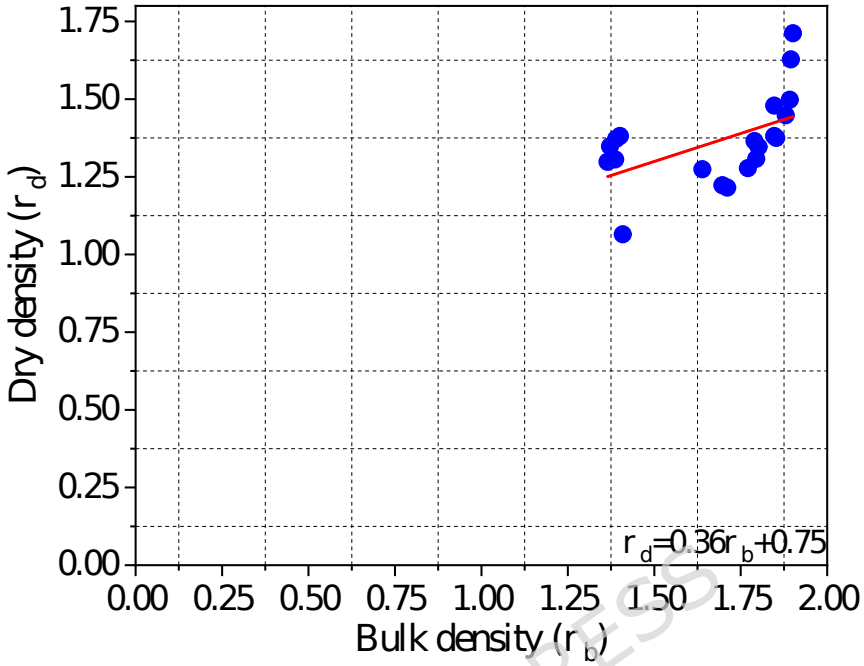

Fig. 12. Bulk density and dry density of soil samples

4.4 Determination of Particle Size Distribution

Particle size distribution (PSD) analysis was performed on 63 soil specimens collected layer-wise, and the percentage of different soils is depicted in the histogram in Fig. 13. The histogram of sample size, correlated with the percent of gravel, revealed that 60 soil samples among 63 samples had a gravel percentage below 50%. Similarly, the histograms for sand, silt, and clay percentages indicated that 57, 15, and 60 soil samples, respectively, had percentages below 50%. The clay content within the soil samples was assessed through hydrometer tests, and the outcomes of these tests are illustrated in Fig. 14. It was found that clay content varied from 0% to 34%. However, after the refusal during the SPT,

the later was recognised as hard clay. In addition, the sample was collected from the hard clay for laboratory testing, it was found that this clay is fine particles with highly natural compacted clay. The PSD analysis results are shown in Fig. 14.

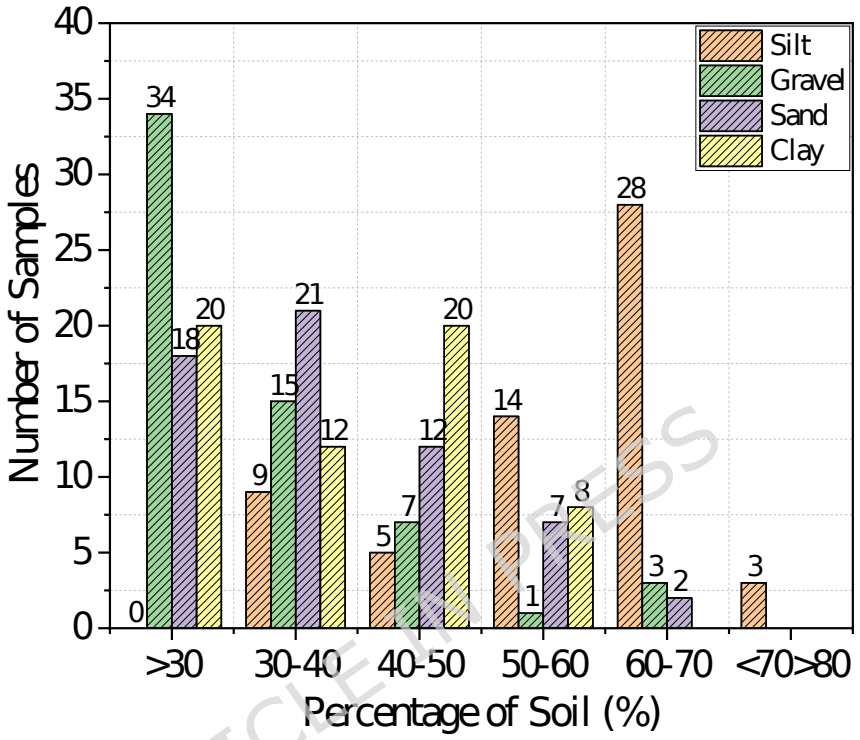

Fig. 13. Histogram stating number of samples with corresponding percentage of soil

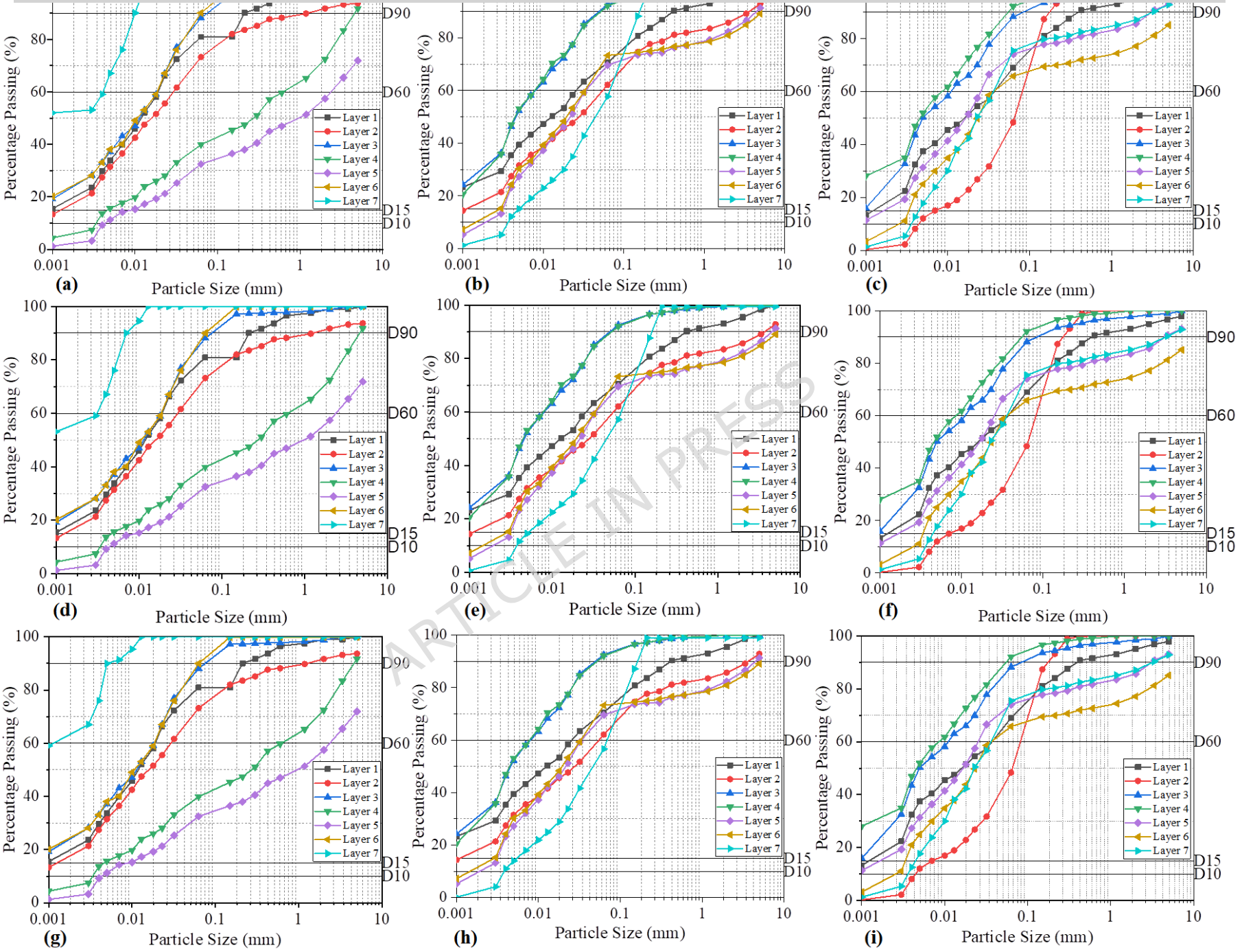

Fig. 14. (a-i) Particle Size Distribution of Soil Samples of 9 Boreholes with Layer Wise Depth

4.5 Determination of Atterberg Limits

Atterberg tests were conducted to determine the liquid limit and plastic limit of the soil sample. The plasticity index was calculated by subtracting the plastic limit from the liquid limit. A total of 44 samples underwent testing, and the results are illustrated in the histogram of Fig. 15(a). Among these samples, the liquid limit of 14 samples was below 50%, while the remaining 30 samples exhibited a liquid limit exceeding 50% and highest was 84%. Consequently, 5 soil samples are categorised as moderately plastic with a range 5% to 15%, whereas the 33 soil samples considered in this study are classified as plastic with a range of 15% to 40%. In addition, 5 samples were categorised as very plastic having greater than 40% PI. The range of liquid limits across all soil samples varied from a minimum of 40% to a maximum of 84%. A plasticity chart is utilised to plot all soil samples, enabling the determination of soil classification based on the USCS classification system shown in Fig. 15(b).

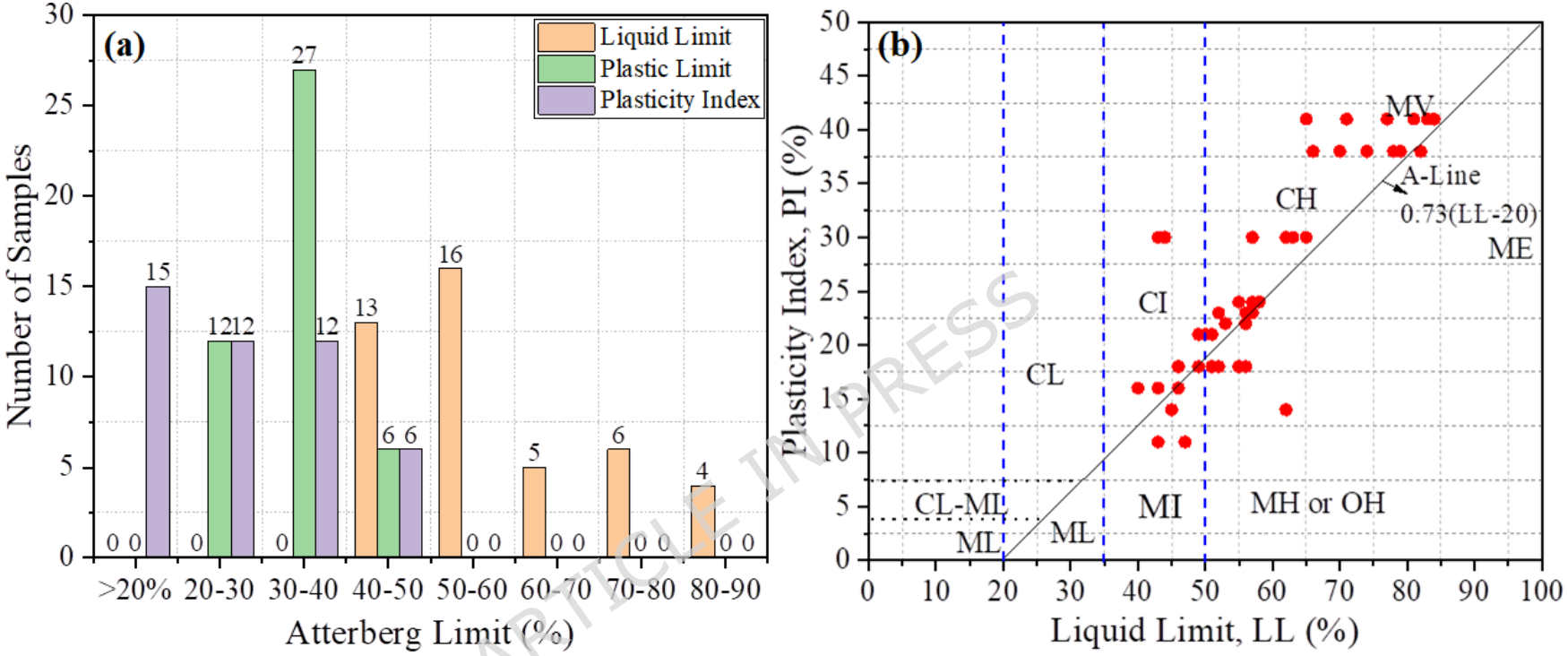

Fig. 15 (a). Distribution of Atterberg Limit of Collected Soil Samples **(b)** Plasticity Chart of Soil Samples in Lubok Antu

One of the central challenges in this study is reconciling bulk resistivity measurements obtained from ERT with the localised geotechnical parameters measured through SPT, shear wave velocity (V_s), and other laboratory tests. In this perspective, the geological characteristics of the Lubok Antu region, dominated by fine-grained soils, particularly clays and silts, and exhibiting a consistent moisture regime, contribute to a reduced heterogeneity in subsurface conditions. These factors are believed to allow ERT measurements to more closely approximate the local mechanical behavior, as the resistivity values reflect more uniform soil behavior across the subsurface layers. This is in contrast to more heterogeneous regions, where large variations in soil composition and moisture content might lead to more significant discrepancies between bulk resistivity and local geotechnical properties. The relationship between ERT-derived resistivity and geotechnical parameters in Lubok Antu is thus influenced by the relatively low variability in the soil composition and moisture content of the region, facilitating the interpretation of bulk resistivity as a reasonable proxy for local soil conditions.

4.2 Simple Regression Analysis of Soil Electrical Resistivity and Index Geotechnical Properties

In statistical analysis of this study, transparency has been ensured by explicitly stating the criteria used to exclude data points from the regression analysis. Data points were excluded if they exhibited significant measurement errors or were affected by local site effects, such as nearby

infrastructure or heterogeneous geological conditions. These exclusions were based on a combination of visual inspection of the data, residual analysis, and sensitivity tests. To improve the robustness of the regression models, this study included confidence intervals around the best-fit lines, which quantify the uncertainty of the correlations and allow for a more reliable interpretation of the results. This study emphasize that the excluded data were outliers that could have skewed the results, and the final statistical models represent the best fit to the core dataset. The simple regression analysis has been carried out between the soil resistivity and key geotechnical parameters and are described as follows. The soil resistivity data and laboratory data has been compiled in the Table 3.

Table 3. The Soil Resistivity Data and Laboratory Data of all the Boreholes

													Atterberg Limit			Particle Size Distribution							
Depth	**Description**	**pH**	**SPT-N value**	**Unit Weight**	V_s	**Linear Shrinkage (%)**	**Bulk Density (Mg/m^3)**	**Dry Density (Mg/m^3)**	**Particle Density**	**Porosity**	**Void Ratio**	**Moisture Content (%)**	**LL (%)**	**PL (%)**	**PI (%)**	**Gravel (%)**	**Sand (%)**	**Silt (%)**	**Clay (%)**	**Classification**	**Specific gravity**	**Degree of saturation**	**Resistivity**
Borehole 1																							
1.50	very Soft Silt	6.2	4	19	140.69	5	1.639	1.274	2.6	0.36961	0.586333	28.61	51	34	18	1	18	61	20	MH	2.6	126.86	103.7
3.00	Soft Silt	5.7	4	19.5	140.69	3.6	1.847	1.381	2.64	0.30037	0.429345	33.8	56	33	23	8	15	55	19	MH	2.64	207.83	186.33
4.50	Stiff Silt	5.7	7	20	166.27	2.9	1.853	1.375	2.68	0.30858	0.446303	34.77	56	34	22	1	11	63	25	MH	2.68	208.78	201.42
7.00	Hard Silt	6.6	8	20.5	173.04	2.9	1.901	1.712	2.55	0.25451	0.341399	11.1	57	35	24	28	33	34	5	MH	2.55	82.90	284.25
9.00	Stiff Clay	6.7	10	18.5	184.96	1.4	1.895	1.628	2.66	0.28759	0.403694	16.43	43	25	30	43	25	30	2	GM	2.66	108.25	250.5
12.00	Clay	5.7	50	18	299.30	2.1	1.88	1.448	2.68	0.29850	0.425532	29.85	62	31	30	0	10	66	24	MH	2.68	187.99	242.12
14.00	Hard clay			20.5		0																	501.76
30.00	Hard Rock			25		0																	949.41
Borehole 2																							
3.00	Soft Silt with Gravel	5.8	2	19	114.41	4.3	1.847	1.479	2.66	0.305639	0.440173	24.85	49	28	21	4	25	42	29	MI	2.66	150.17	79.43
7.50	Soft Silt with Gravel	6.1	4	19	140.69	4.3	1.79	1.365	2.63	0.319392	0.469274	31.15	46	27	18	14	24	33	29	MI	2.63	174.57	100
8.00	Stiff Silt	4.4	4	20	140.69	2.9	1.711	1.215	2.67	0.359176	0.560491	40.84	74	36	38	0	7	59	34	MV	2.67	194.54	186.33
9.50	Stiff Silt	4.3	9	20	179.23	3.6	1.697	1.223	2.6	0.347308	0.532115	38.77	77	36	41	0	8	61	31	MV	2.6	189.43	284.25
10.50	Stiff Silt	5.2	10	20	184.96	1.4	1.387	1.306	2.67	0.480524	0.925018	6.21				18	13	59	10	M	2.67	17.92	340.76
13.50	Stiff Silt	5.0	11	20	190.30	1.4	1.365	1.298	2.66	0.486842	0.948718	5.23				19	8	61	12	M	2.66	14.66	501.19
17.00	Hard Silt	6.2	50	20.5	299.30	2.1	1.771	1.278	2.72	0.348897	0.535855	38.69	45	31	14	0	42	54	4	MI	2.72	196.39	501.19
30.00	Hard Rock			25		0																	676.73
Borehole 3																							
2.00	Soft Silt	6.3	4	19.5	140.69	3.6	1.892	1.498	2.65	0.286038	0.400634	26.26	43	27	16	5	26	50	19	MI	2.65	173.69	101.25
3.50	Soft Silt	6.5	5	19.5	150.38	3.6	1.795	1.308	2.74	0.344891	0.526462	37.29	43	32	11	0	48	37	15	MI	2.74	194.07	185.96
5.00	Soft Silt	4.5	6	19.5	158.79	2.9	1.802	1.346	2.75	0.344727	0.526082	33.83	83	43	41	1	10	61	28	MV	2.75	176.84	284.35
7.50	Soft Silt	4.3	7	19.5	166.27	1.4	1.409	1.065	2.7	0.478148	0.916253	32.25	79	40	38	0	8	60	32	MV	2.7	95.03	340.8
9.00	Stiff Silt	4.9	15	20	208.79	1.4	1.372	1.348	2.65	0.482264	0.931487	1.76				14	12	58	16	M	2.65	5.007	501.19

10.50	Stiff Silt	5.7	17	20	216.75	2.1	1.39	1.372	2.71	0.487085	0.94964	1.29				23	11	59	7	M	2.71	3.68	501.19
14.00	Hard Silt	5.3	50	20.5	299.30	1.4	1.401	1.381	2.68	0.477239	0.912919	1.47				13	12	71	4	M	2.68	4.31	501.19
Borehole 4																							
1.50	very Soft Silt	6.2	4	19	140.69	5	1.56	1.474	2.5	0.376	0.602564	30.15	52	34	18	2	17	62	19	MH	2.6	130.09	113.2
3.00	Soft Silt	5.8	5	19.5	150.38	3.6	1.81	1.581	2.54	0.287402	0.403315	35.34	57	33	23	9	14	56	18	MH	2.64	231.32	186.33
4.50	Stiff Silt	5.6	8	20	173.04	2.9	1.853	1.575	2.58	0.281783	0.392337	36.31	56	34	22	2	10	64	24	MH	2.68	248.02	201.42
7.00	Hard Silt	6.7	10	20.5	184.96	2.9	1.92	1.912	2.45	0.216327	0.276042	12.64	58	35	24	29	32	35	4	MH	2.55	116.76	289.55
9.00	Stiff Clay	6.7	15	18.5	208.79	1.4	1.902	1.828	2.59	0.265637	0.361725	17.97	44	25	30	44	24	31	1	GM	2.66	132.14	250.5
12.00	Clay	5.8	50	18	299.30	2.1	1.899	1.648	2.61	0.272414	0.374408	31.39	63	31	30	1	9	67	23	MH	2.68	224.68	242.12
14.00	Hard Silt	5.5		20.5		0																	340.76
30.00	Hard Rock			25		0																	500.15
Borehole 5																							
3.00	Soft Silt with Gravel	5.8	4	19	140.696	4.3	1.866	1.679	2.55	0.268235	0.366559	27.46	50	28	21	5	24	43	28	MI	2.66	199.41	95.6
7.50	Soft Silt with Gravel	6.1	6	19	158.796	4.3	1.83	1.565	2.53	0.27668	0.382514	38.51	55	27	18	15	23	34	28	MI	2.63	264.77	100
8.00	Stiff Silt	4.3	9	20	179.236	2.9	1.722	1.415	2.57	0.329961	0.492451	35.05	78	36	38	1	6	60	33	MV	2.67	190.03	250.34
9.50	Stiff Silt	4.3	11	20	190.309	3.6	1.712	1.423	2.5	0.3152	0.46028	33.47	81	36	41	1	7	62	30	MV	2.6	189.06	284.25
10.50	Stiff Silt	5.3	15	20	208.791	1.4	1.421	1.506	2.57	0.447082	0.808586	2.98				19	12	60	9	M	2.67	9.84	413.51
13.50	Stiff Silt	5.0	25	20	243.242	1.4	1.41	1.498	2.55	0.447059	0.808511	2.51				20	7	62	11	M	2.66	8.25	501.19
17.00	Hard Silt	6.1	50	20.5	299.301	2.1	1.82	1.478	2.62	0.305344	0.43956	2.69	45	31	14	1	41	55	3	MI	2.72	16.64	501.19
30.00	Hard Rock			25		0																	798.33
Borehole 6																							
2.00	Soft Silt	6.2	5	19.5	150.385	3.6	1.911	1.698	2.55	0.250588	0.33438	25.81	46	27	16	6	25	51	18	MI	2.65	204.54	123.95
3.50	Soft Silt	6.5	7	19.5	166.276	3.6	1.813	1.508	2.64	0.313258	0.45615	36.84	47	32	11	1	51	48	0	MI	2.74	221.29	191.56
5.00	Soft Silt	4	9	19.5	179.236	2.9	1.821	1.546	2.65	0.31283	0.455244	33.38	84	43	41	2	9	62	27	MV	2.75	201.63	284.35
7.50	Soft Silt	4.3	13	19.5	200.049	1.4	1.422	1.265	2.6	0.453077	0.828411	31.8	82	40	38	1	7	61	31	MV	2.7	103.64	386.78
9.00	Stiff Silt	5.0	15	20	208.791	1.4	1.391	1.548	2.55	0.45451	0.833214	1.31				15	11	59	15	M	2.65	4.16	408.91
10.50	Stiff Silt	5.6	19	20	224.078	2.1	1.415	1.572	2.61	0.457854	0.844523	0.84				24	10	60	6	M	2.71	2.69	501.19
14.00	Hard Silt	5.2	50	20.5	299.301	1.4	1.426	1.581	2.58	0.447287	0.809257	1.02				14	11	72	3	M	2.68	3.37	501.19

30.00	Rock																					835.1
Borehole 7																						
1.50	very Soft Silt	6.1	3	19	129.125	5	1.692	1.255	2.7	0.373333	0.595745	29.35	49	34	18	3	16	63	18	MH	2.6	128.09	131.15
3.00	Soft Silt	5.6	5	19.5	150.385	3.6	1.947	1.362	2.74	0.289416	0.407293	34.54	52	33	23	10	13	57	17	MH	2.64	223.88	186.33
4.50	Stiff Silt	5.8	7	20	166.276	2.9	1.925	1.356	2.78	0.307554	0.444156	35.51	53	34	22	3	9	65	23	MH	2.68	214.26	224.32
7.00	Hard Silt	6.5	8	20.5	173.04	2.9	1.951	1.693	2.65	0.263774	0.358278	11.84	55	35	24	30	31	36	3	MH	2.55	84.26	284.25
9.00	Stiff Clay	6.9	16	18.5	212.857	1.4	1.912	1.609	2.77	0.309747	0.448745	17.17	57	25	30	45	23	32	0	GM	2.66	101.77	250.5
12.00	Clay	5.9	50	18	299.301	2.1	1.9	1.429	2.78	0.316547	0.463158	30.59	65	31	30	2	8	68	22	MH	2.68	177.00	242.12
14.00	Hard Silt	6.1		20.5		0																	500.51
30.00	Hard Rock			25		0																	936.45
Borehole 8																						
3.00	Soft Silt with Gravel	5.7	5	19	150.385	4.3	1.88	1.46	2.63	0.285171	0.398936	24.85	51	28	21	6	23	44	27	MI	2.66	165.69	98.67
7.50	Soft Silt with Gravel	6.2	8	19	173.04	4.3	1.82	1.346	2.6	0.3	0.428571	31.15	56	27	18	16	22	35	27	MI	2.63	191.15	118.98
8.00	Stiff Silt	4.5	8	20	173.04	2.9	1.75	1.196	2.64	0.337121	0.508571	40.84	70	36	38	2	5	61	32	MV	2.67	214.41	186.33
9.50	Stiff Silt	4.4	9	20	179.236	3.6	1.71	1.204	2.57	0.33463	0.502924	38.77	71	36	41	2	6	63	29	MV	2.6	200.43	303.45
10.50	Stiff Silt	5.2	15	20	208.791	1.4	1.42	1.287	2.64	0.462121	0.859155	6.21				20	11	61	8	M	2.67	19.29	340.76
13.50	Stiff Silt	5.2	18	20	220.485	1.4	1.45	1.279	2.66	0.454887	0.834483	5.23				21	6	63	10	M	2.66	16.67	487.51
17.00	Hard Silt	6.3	50	20.5	299.301	2.1	1.88	1.259	2.69	0.301115	0.430851	38.69	65	31	14	2	40	56	2	MI	2.72	244.25	501.19
30.00	Hard Rock			25		0																	921.45
Borehole 9																						
2.00	Soft Silt	6.4	5	19.5	150.385	3.6	1.9	1.479	2.62	0.274809	0.378947	27.21	40	27	16	7	24	52	17	MI	2.65	190.28	179.54
3.50	Soft Silt	6.5	7	19.5	166.276	3.6	1.89	1.289	2.69	0.297398	0.42328	38.24	43	32	11	2	50	49	-1	MI	2.74	247.53	185.96
5.00	Soft Silt	4.4	11	19.5	190.309	2.9	1.9	1.327	2.72	0.301471	0.431579	34.78	65	43	41	3	8	63	26	MV	2.75	221.61	296.85
7.50	Soft Silt	4.4	14	19.5	204.529	1.4	1.5	1.046	2.67	0.438202	0.78	33.2	66	40	38	2	6	62	30	MV	2.7	114.92	340.8
9.00	Stiff Silt	4.9	15	20	208.791	1.4	1.41	1.329	2.61	0.45977	0.851064	2.71				16	10	60	14	M	2.65	8.43	467.84
10.50	Stiff Silt	5.8	17	20	216.75	2.1	1.45	1.353	2.68	0.458955	0.848276	2.24				25	9	61	5	M	2.71	7.15	491.25
14.00	Hard Silt	5.4	50	20.5	299.301	1.4	1.5	1.362	2.65	0.433962	0.766667	2.42				15	10	73	2	M	2.68	8.45	501.19
	Rock			25																			867.41

4.2.1 Correlation between Resistivity and Shear Wave Velocity (V_s)

The velocity of shear wave propagation, V_s, is a key soil property, used for soil characterisation, such as the estimation of small-strain shear modulus, liquefaction resistance, seismic response, and assessment of the effectiveness of soil improvement methods used in soils, as well as others. The specific soil-type relationships such as, Imai and Tonouchi (1982), Ohta and Goto (1977), Hasancebi and Ulusay (2007) shown in Table 1 has been used to calculate the V_s in the Lubok Antu region of Sarawak by following the methodology of (Nabilah et al., 2023). This V_s has been calculated using the SPT-N values. The V_s profiles obtained from the simple regression at specific locations near the resistivity tests were used to develop correlations between resistivity and shear wave velocity. The variation of V_s with depth is shown in Fig. 16(a), the resistivity and V_s values were considered for developing the correlations is shown in Fig. 16(b). Where an increase in resistivity was found to result in an increase in shear wave velocity. A linear relationship was observed between the two parameters, with a regression coefficient (R^2) of 0.62 indicating a strong correlation. The equation between shear wave velocity and resistivity is shown in. Some erroneous values were omitted from the dataset due to measurement errors and local site effects.

$$Vs = 0.2238\rho + 132.07 \quad (4)$$

The regression plots presented in this study include confidence intervals around the best-fit lines, calculated using standard error of the regression coefficients. These intervals provide insight into the uncertainty of the

estimated relationships between resistivity and the geotechnical parameters. The confidence intervals help quantify the variability in the data and offer a clearer assessment of the robustness of the correlations.

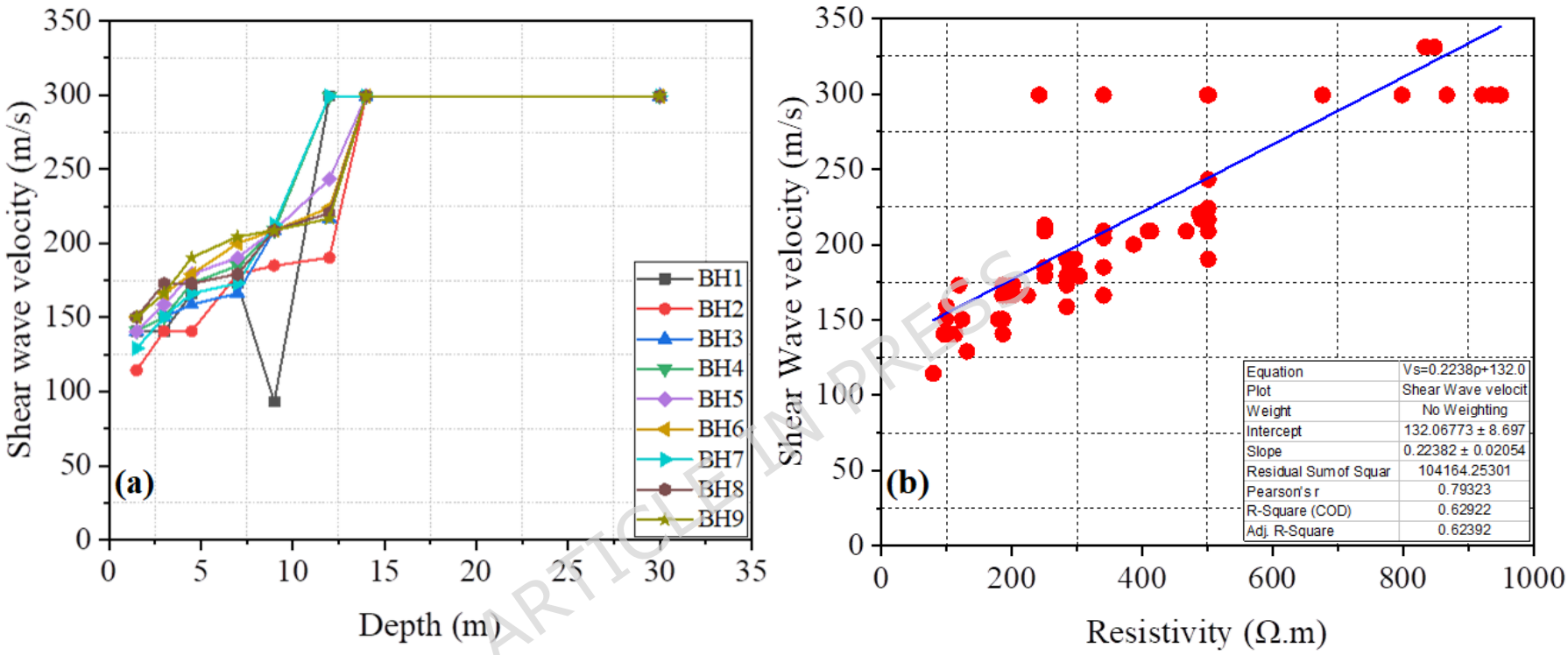

Fig. 16. (a) The Variation of Shear Wave Velocity with Depth **(b)** Correlation between Resistivity and Shear Wave Velocity

4.2.2 Correlation between Resistivity and SPT - N

The Fig. 17 illustrates the variation of SPT - N over the depth up to 30m in the Lubok Antu region. Generally, SPT - N values increase with depth up to 10-15 meters and then SPT - N values beyond 50 were considered as refusal and SPT is terminated and not used for correlation development. The resistivity values also showed a similar trend with depth. The water table depth in the area is approximately 10 meters, and the resistivity values beyond the water table were affected by its presence. Therefore, the resistivity and SPT - N values up to 10 meters were used to develop the correlations.

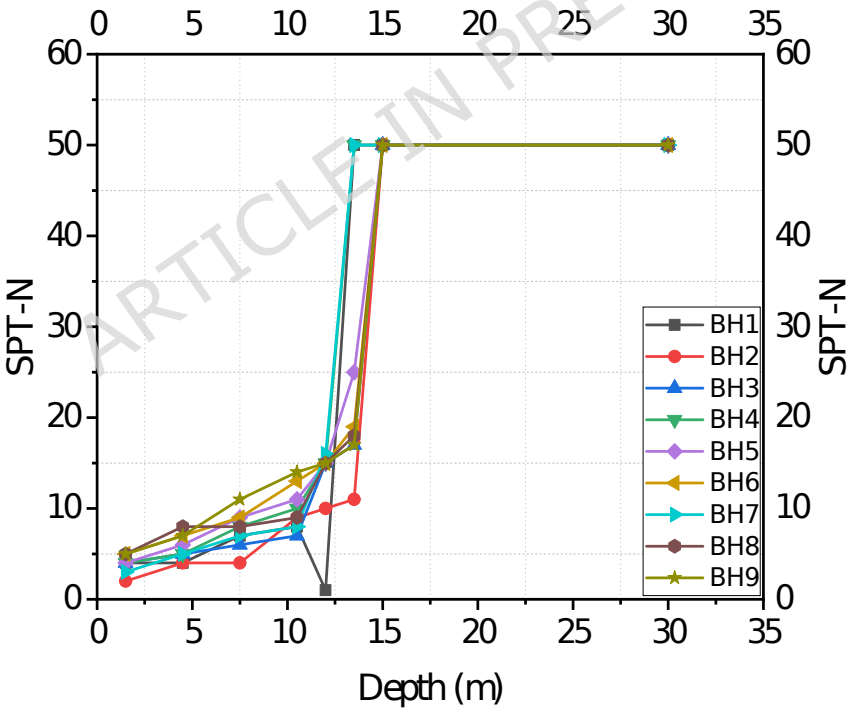

Fig. 17. Depth versus SPT-N

Fig. 18 shows the relationship between resistivity and SPT - N. A linear relationship was observed between the two parameters with a regression

coefficient (R^2) of 0.55, indicating a medium correlation between SPT - N and soil resistivity (ρ) and the equation is shown in (5. However, the coefficients in the linear relations are sensitive to the clay content and lithology at the site. Some of the measurement errors were excluded from the dataset to develop the correlations, which slightly reduced the R^2 value.

$$N = 0.0636\rho - 1.7577 \quad (5)$$

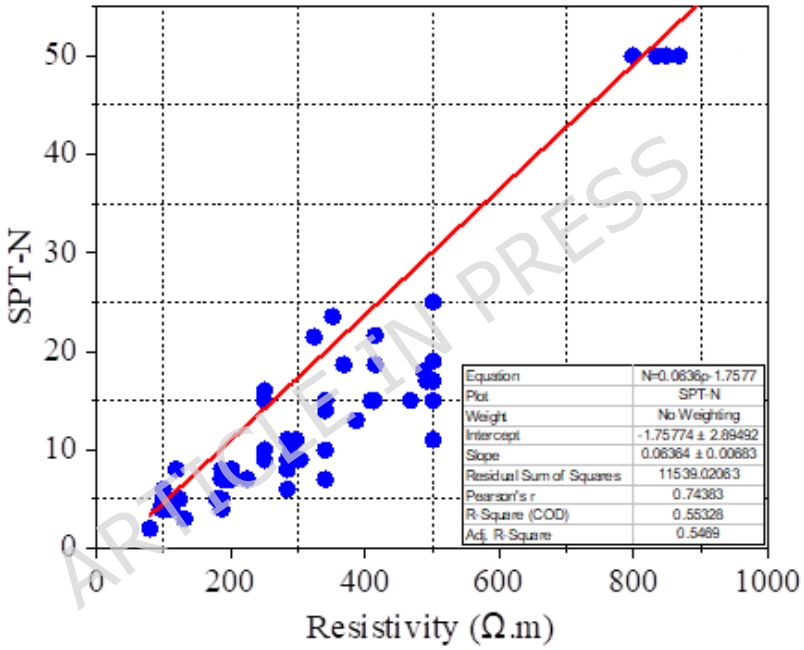

Fig. 18. Resistivity Correlation with SPT-N

4.2.3 Correlation between Resistivity and Moisture Content

The moisture content of the soil has a significant impact on its resistivity, and to examine this effect, a correlation was established. This correlation was developed by conducting resistivity tests at a particular depth of 1 meter beneath the ground surface at the same location while varying the moisture content. The tests were conducted each day following occasional

rainfall until there was no further alteration in resistivity. After the test, samples were gathered using a core cutter, and the moisture content was determined in the laboratory. The depth-wise resistivity is shown in Fig. 19(a). There is a strong relationship between the resistivity and moisture content with R^2 of 0.74 shown in Fig. 19(b). In addition the equation between the resistivity and moisture content is shown in (6.

$$\rho = 592.4w^{-0.226} \quad (6)$$

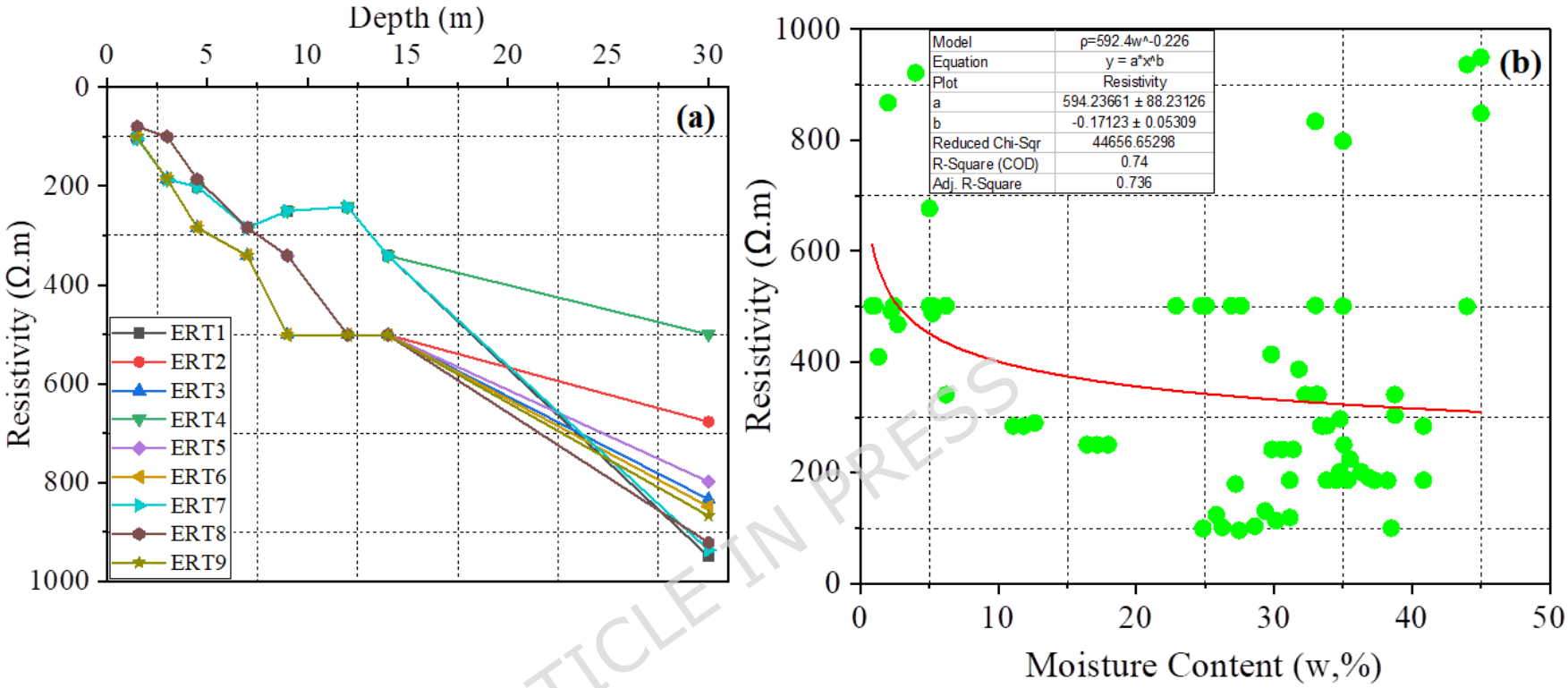

Fig. 19. (a) Depth versus Resistivity (b) Correlation between Resistivity and Moisture Content

In Fig. 19(b), the relationship between resistivity and moisture content is displayed. The results show that as moisture content increases, the resistivity of the soil (ρ) decreases. The correlation between resistivity and moisture content was observed to be nonlinear and followed a power relationship with a regression coefficient of 0.74, as presented. Previous research by Pozdnyakov et al., (2006) suggested that water significantly impacts the mobility of electrical charge in soil. With higher moisture content, electrical current can be conducted through the pore water (Siddiqui & Osman, 2013). The correlation presented in this study exhibits similarities to those reported in previous research (Hatta & Osman, 2015; Hegde & Anand, 2022; Rezaei et al., 2018; Siddiqui & Osman, 2013; Zhang et al., 2018).

It is revealed from this research that that high moisture content (20-40%) corresponds to low resistivity (80-200Ω.m), low moisture content (1-6%) corresponds to high resistivity (300-500 Ω.m) and hard rock shows very high resistivity (500-950 Ω.m) with negligible moisture. While the geophysical resistivity measurements provide a bulk representation of subsurface properties, the geotechnical parameters like SPT-N and moisture content reflect more localised characteristics. This scale mismatch necessitates careful consideration when applying these correlations to large-scale geotechnical site characterisation.

Table 4. Assessing how the Proposed Correlation compares to Prior Research

S.no	Authors	Data pairs		Location	Correlation	R^2
		SPT	ERT			
01	Braga et al., (1999)	49	06	São Paulo	$N = \left(\rho/_{6839.72}\right)0.70$	0.70
02	Liu et al., (2008)	Laboratory		China	$N = 2.3\rho + 2.7$	0.82
03	Oh & Sun (2008)	05	06	South Korea	$\rho = 18.5N$	0.47
04	Hatta & Osman (2015)	11	03	Perak, Malaysia	$\rho = 20.94N + 281.56$	0.90
05	Zhang et al., (2018)	06	06	Jiangsu, China	$\rho = 53.8Cs^{-0.85}$	0.83
06	Rezaei et al., (2018)	06	06	Nargeschal, Golestan	$\rho = 15.65e^{0.034N}$	0.55

07	Hegde & Anand (2022)	16	16	Patna, India	$N = 0.1049\rho - 3.1576$	0.62
					$N = 0.0636\rho - 1.175$	0.55
08	Present study	09	09	Lubok Antu, Sarawak	$\rho = 592.4w^{-0.226}$	0.74
					$pH = 0.002\rho + 5.6101$	0.58
					$V_s = 0.2238\rho + 132.07$	0.62
					$k = -0.0018\rho + 1.5758$	0.76
					$\rho = 284.75e^{0.65}$	0.71
					$\rho = 20.363PI^{0.704}$	0.72

The newly developed correlations were found to be consistent with many of the previously conducted studies (Hatta & Osman, 2015; Hegde & Anand, 2022; Liu et al., 2008; Oh & Sun, 2008). Table 4 provides a comparison of the correlation results obtained in this study with those of

earlier research. Depending on the soil type, various types of correlations were observed between the SPT - N and soil resistivity (ρ), such as linear, power, exponential, etc. The present study showed the highest value of the regression coefficient (R^2) as compared to previous research. Therefore, the linear relationship between SPT-N and resistivity is strongly supported for the soil in Lubok Antu region of Sarawak, Malaysia.

The moisture content of soil has a significant impact on its resistivity. Coelho et al., (2015) found that soil resistivity and ground resistance can vary significantly with changes in moisture content, which can affect the performance of grounding systems. Beck et al., (2011) further demonstrated a linear relationship between resistivity and dry density, with the sensitivity decreasing as water content increases. Butalia et al., (2003) and Bertermann and Schwarz (2018) both highlighted the decrease in soil strength and stiffness with increased moisture content, with Butalia specifically noting a decrease in resilient modulus. Bertermann also developed a soil texture-independent relation between electrical conductivity and soil moisture content. These studies collectively underscore the importance of considering moisture content in soil resistivity measurements and the design of grounding systems.

4.2.4 Correlation between Resistivity and pH

A linear relationship was observed between the two parameters with a regression coefficient (R^2) of 0.58, indicating a medium correlation between pH value and soil resistivity (ρ), and the equation is provided in (7 shown in Fig. 20. However, the coefficients in the linear relations are

sensitive to the peak ground acceleration (PGA), the nature of the seismic wave, the duration of the event, and the lithology at the site. Some of the measurement errors were excluded from the dataset to develop the correlations, which slightly reduced the R^2 value.

$$pH = 0.002\rho + 5.6101 \quad (7)$$

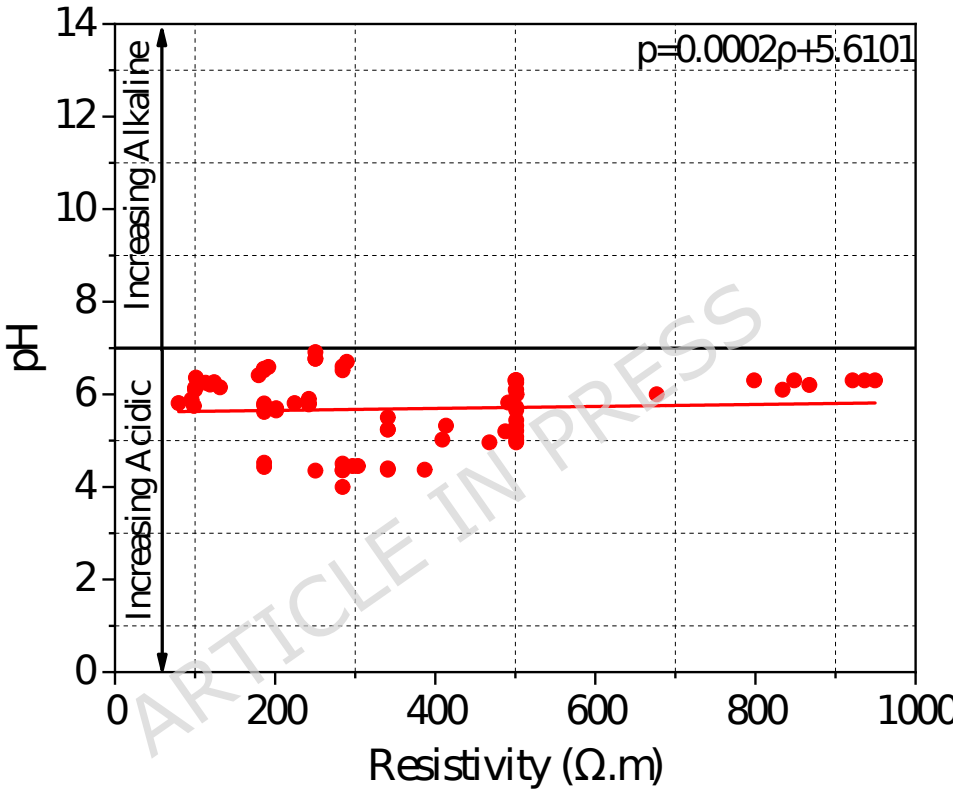

Fig. 20. Correlation between Resistivity and pH

4.2.5 Correlation between Resistivity and Hydraulic Conductivity

To accurately anticipate and control soil instabilities, it is essential to establish a connection between the hydrogeological characteristics of the soil and its electrical properties. This necessitates a comprehensive understanding of both the hydraulic conductivity and the electrical resistivity of the soil. The subsurface movement of water is contingent on

the soil's hydraulic conductivity, representing the ease with which water or fluid traverses the pore spaces within the soil. The change in hydraulic conductivity concerning change in depth is shown in Fig. 21.

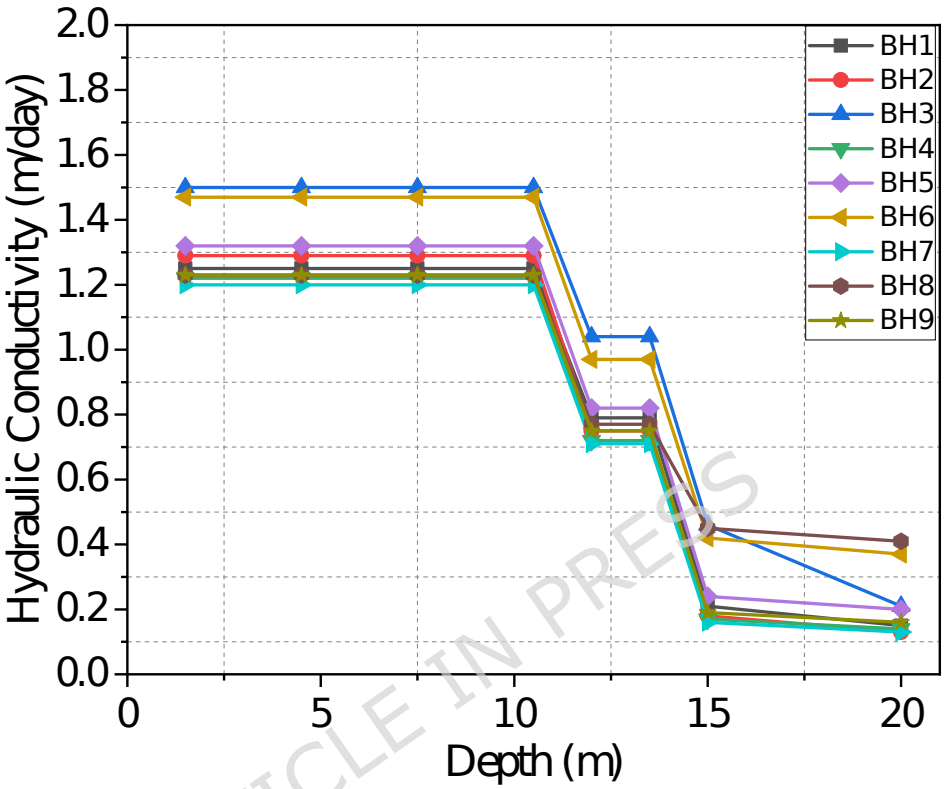

Fig. 21. Hydraulic Conductivity with respect to Depth

This flow or movement of soil water hinges on the porosity of soils, being more prominent in coarse-grained soil (such as sand) compared to fine-grained soil (such as clay). The hydraulic conductivity of the soil is influenced by seasonal fluctuations in soil water content. Consequently, a thorough understanding of soil hydraulic conductivity is crucial for evaluating slope instability in residual soil. The findings indicated that hydraulic conductivity values can be derived from electrical resistivity data, particularly when there is pertinent information from borehole penetration tests. It was found from the results that hydraulic conductivity

decreases as the depth increases. Also, Fig. 22(a) and Fig. 22(b) illustrate the correlation between resistivity and hydraulic conductivity. It was found that resistivity is inversely proportional to hydraulic conductivity; resistivity increases, and hydraulic conductivity decreases, indicating the presence of clay content.

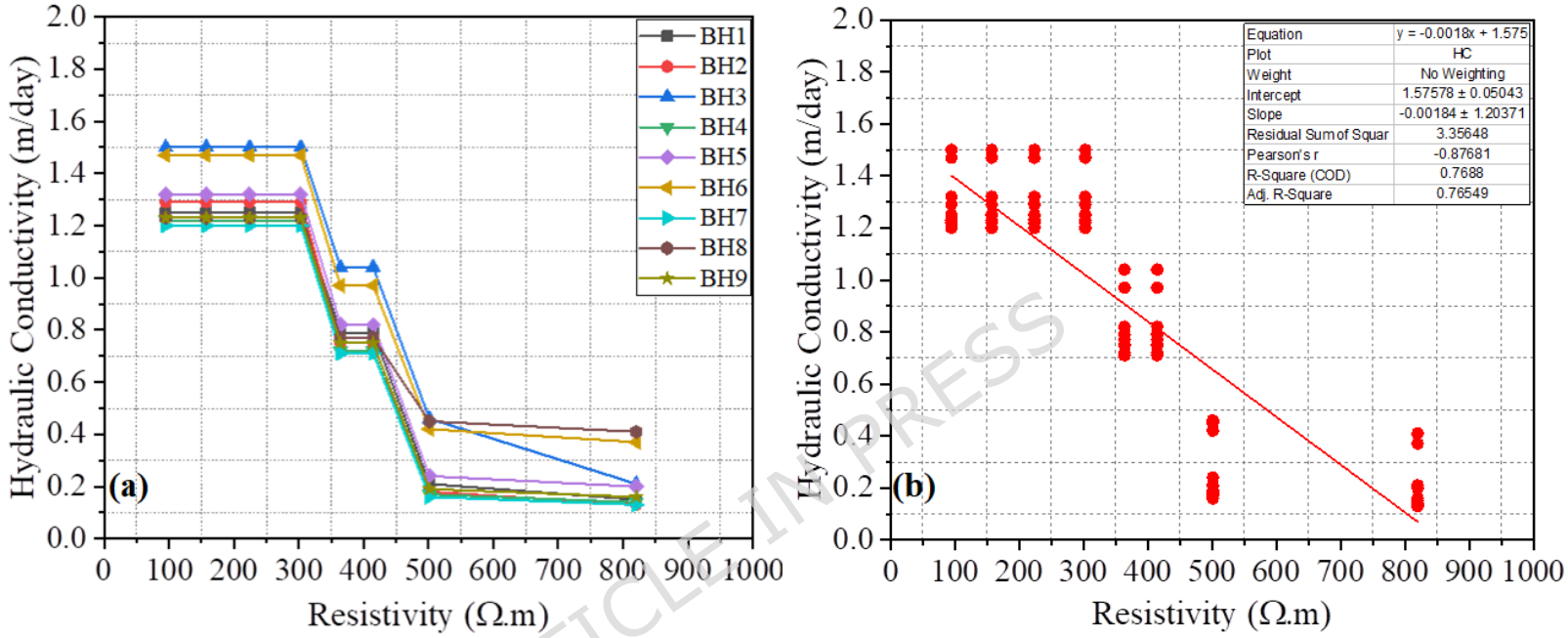

Fig. 22. (a) Resistivity and Hydraulic Conductivity (b) Correlation between Resistivity and Hydraulic Conductivity

A linear relationship was observed between the two parameters with a regression coefficient (R^2) of 0.76, indicating a strong correlation between hydraulic conductivity and soil resistivity (ρ) and the equation is provided in (8. However, the coefficients in the linear relations are sensitive to the clay content and lithology at the site.

$$k = -0.0018\rho + 1.5758 \quad (8)$$

4.2.6 Correlation between Void Ratio and Resistivity

A significant exponential relationship was observed between void ratio and soil resistivity (R^2=0.71), following equation $\rho = 284.75e^{0.65}$. This correlation indicates the soil porosity exerts a substantial influence on electrical properties, with higher void ratios corresponding to increased resistivity values across all soil types in the Lubok Antu formation. The strong positive correlation between void ratio and resistivity reveals fundamental insights into the pore structure's role in electrical conduction. Higher void ratios typically indicate better-drained, more porous soils where conductive pore water phase becomes discontinuous, leading to increased resistivity. Conversely, lower void ratios characterised denser soils with reduced porosity and potentially higher saturation, facilitating better electrical conductivity through the pore network.

This relationship is particularly evident in the transition from soft silts (void ratio ≈ 0.4-0.6, resistivity ≈ 100-200Ω.m) to stiff/hard silts (void ratio ≈ 0.8-0.95, resistivity ≈ 300-500Ω.m). The exponential nature of the correlation suggests that small changes in porosity at higher void rations

result in disproportionately large changes in resistivity, highlighting the sensitivity of electrical methods to soil compaction state.

For practical implications, the void ratio-resistivity correlation enables preliminary assessment of soil density and compaction state from ERT surveys. Areas showing higher resistivity may indicate looser, more compressible soils requiring additional geotechnical investigations, while lower resistivity zones likely represent denser, more competent materials.

4.2.6 Correlation between Plasticity Index and Resistivity

The relationship between Plasticity Index (PI) and electrical resistivity reveals a significant, non-linear trend controlled by the competing influences of clay mineralogy and soil state shown in Fig. 32. Soils with moderate PI values (20-30%), typically representing clays and silty clays, exhibit the lowest resistivity (approximately 200-250 Ω·m). This is attributed to the dominance of surface conductivity, where the high specific surface area and cation exchange capacity of clay minerals provide a highly conductive pathway. However, this trend reverses for soils with very high PI (>35), which correspond to stiffer, more consolidated layers that often have lower natural moisture contents and a more flocculated fabric, reducing pore connectivity. As a result, these high-PI soils have an unexpectedly high resistivity (300-500 m), indicating that the overall soil fabric and saturation state ultimately control the bulk electrical response, despite the fact that clay content typically increases conductivity.

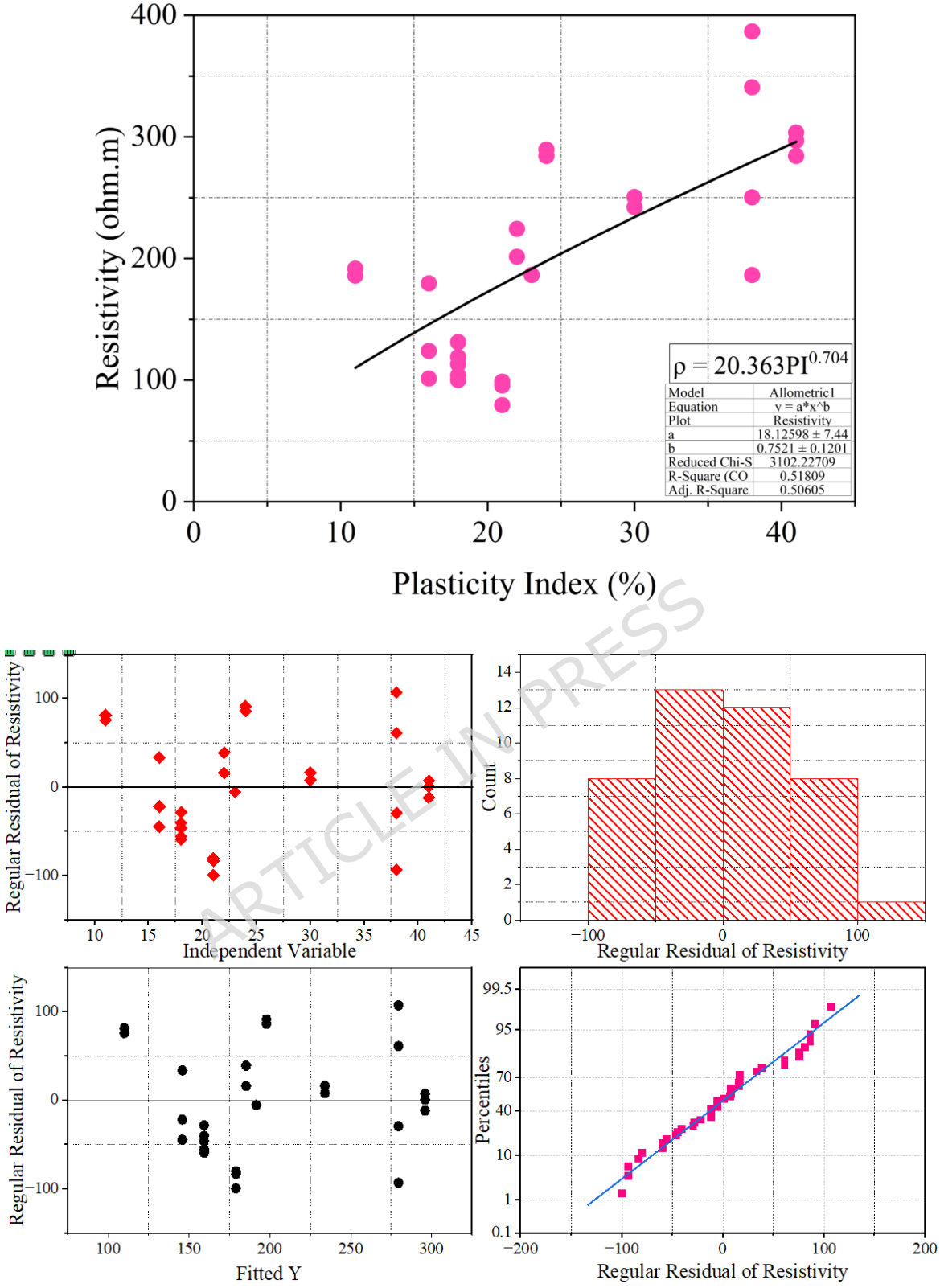

Fig. 23. Correlation between Plasticity Index and Resistivity of Soil

4.3 Scale Mismatch and Data Integration

It is essential to acknowledge the inherent scale mismatch between bulk geoelectrical resistivity measurements, which provide a macroscopic view of subsurface properties, and the highly localised nature of geotechnical indices such as SPT-N, Atterberg limits, moisture content, and hydraulic conductivity. This scale discrepancy can limit the direct applicability of the correlations across different geological settings. Therefore, future studies may consider using higher-resolution geophysical techniques or complementary geotechnical methods to refine the correlations further.

4.4 Geological context and Scale Mismatch

The Lubok Antu region is characterised by a fine-grained soil matrix, with clay and silt being the dominant components. This composition, coupled with the region's consistent moisture regime, significantly reduces subsurface heterogeneity. As a result, the bulk resistivity measurements from ERT are more likely to reflect the local mechanical behavior, even though ERT and geotechnical measurements inherently represent different spatial scales. This geological consistency helps explain why moderate-to-high statistical correlations are observed between resistivity and geotechnical parameters, making these correlations not just empirical but grounded in the physical characteristics of the region

5. Conclusions and Future Work

i. This study established robust site-specific correlations between Electrical Resistivity Tomography (ERT) and key geotechnical parameters, such as shear wave velocity (V_s), soil moisture content

(□), and Standard Penetration Test (SPT) blow counts, for the Lubok Antu region in Sarawak, Malaysia.

ii. The correlations developed in this study offer a site-specific approach to subsurface characterisation in the Lubok Antu region. However, their applicability in other regions with different geological and soil conditions requires independent validation.

iii. A strong nonlinear correlation was observed between soil resistivity (ρ) and moisture content (□), with an R^2 value of 0.74, providing a reliable method for estimating soil moisture from resistivity data.

iv. Moderate correlations were found between resistivity and shear wave velocity (R^2 = 0.62), as well as resistivity and SPT-N values (R^2 = 0.55), which can aid in subsurface characterisation and geotechnical site assessment.

v. The integration of ERT with geotechnical testing techniques offers a practical and cost-effective alternative to traditional drilling methods, reducing the need for extensive boreholes and speeding up site assessments.

vi. This work is innovative in its development of region-specific correlations for Lubok Antu, filling a gap in the literature and offering a new approach for subsurface investigations in complex geological settings.

vii. The findings of this study have significant implications for seismic hazard assessments, foundation design, and groundwater exploration, especially in tectonically active regions.

viii. Further validation of these correlations in other regions with similar soil types and geological conditions is recommended to enhance their broader applicability.

ix. Future studies should focus on validating these correlations in other regions with varying lithological and environmental conditions. Further research should also explore additional geophysical techniques to complement ERT for more accurate geotechnical property estimation.

Nomenclatures

List of acronyms	
AB/2	Maximum electrode separation
ANN-PSO	Artificial Neural Network-Particle Swarm Optimisation
C1 and C2	Outer electrodes
EC	Electrical Conductivity
ERT	Electrical resistivity tomography
GIS	Geographic information system
P1 and P2	Inner electrodes
RMS	Root Mean Square
SPT	Standard penetration test
USCS	Unified Soil Classification System
UNIMAS	Universiti Malaysia Sarawak
Latin letters	
ρ	Resistivity (Ω.m)

PI	Plasticity Index (%)
V_s	Shear wave velocity (m/s)
w	Moisture content (%)
k	Hydraulic conductivity (m/day)
pH	Power of hydronium ions
ΔV	Voltage difference (V)
I	Applied current (A)
K	Geometric constant
R^2	Coefficient of determination
σ	Electrical conductivity (S/m)
Greek letters	
ΔT	Temperature difference (°C)
λ	Wavelength (m)
μ	Poisson's ratio (dimensionless)

Acknowledgment

The authors would like to express our sincere gratitude for the financial support provided by the industrial Grant from Multimur Aktif Unggul under grant number IRG/F02/MAUJV/86676/2025, which has enabled the completion of this research.

Data Availability

The datasets used and/or analysed during the current study are available from the corresponding author on reasonable request.

Author contributions

Imtiyaz; Conceptualisation, Writing–original drafting, Methodology, Investigation, **Raudhah;** Supervision, **Raghad;** Supervision, Writing–review & editing, **Nadeem;** Writing–review & editing, **Retinder;** Validation, Writing–review & editing, **Yunika;** Resources, Supervision, **Dayangku;** Data curation, Resources, **Azrin;** Equipment, **Haythem, Nouh and Shaiza;** Writing–review & editing.

Declaration of Competing Interest

There is no conflict of interest

Declaration of generative AI and AI-assisted technologies in the manuscript preparation process

During the preparation of this work the authors used Quillbot and Grammarly in order to enhance the readability of this manuscript. After using this tool/service, the authors reviewed and edited the content as needed and take full responsibility for the content of the published article.

References

Abbas, H. A., Al-Jeznawi, D., Al-Janabi, M. A. Q., Bernardo, L. F. A., & Jacinto, M. A. S. C. (2024). Exploring Shear Wave Velocity—N SPT Correlations for Geotechnical Site Characterization: A Review. *CivilEng*, *5*(1), 119-135.

Ahmad, A. Bin, Ahmadi, R., Najar, I. A., & Abidin, A. S. Z. (2024). Comprehension of Energy-Based Methods for Investigating Soil Suffusion Uncertainties. *International Journal of Design and Nature*

and Ecodynamics, *19*(3), 733–743. https://doi.org/10.18280/ijdne.190303

Akingboye, A. S. (2025). Electrical and seismic refraction methods : Fundamental concepts , current trends , and emerging machine learning prospects. *Discover Geoscience Review*, *3*(87), 1–42. https://doi.org/10.1007/s44288-025-00169-8.

Akin, M. K., Kramer, S. L., & Topal, T. (2011). Empirical correlations of shear wave velocity (Vs) and penetration resistance (SPT-N) for different soils in an earthquake-prone area (Erbaa-Turkey). *Engineering geology*, *119*(1-2), 1-17.

Alamry, A. S., van der Meijde, M., Noomen, M., Addink, E. A., van Benthem, R., & de Jong, S. M. (2017). Spatial and temporal monitoring of soil moisture using surface electrical resistivity tomography in Mediterranean soils. *Catena*, *157*, 388-396.

Alel, M. N. A., Upom, M. R. A., Abdullah, R. A., & Abidin, M. H. Z. (2018, April). Estimating SPT-N value based on soil resistivity using hybrid ANN-PSO algorithm. In *Journal of Physics: Conference Series* (Vol. 995, No. 1, p. 012035). IOP Publishing.

Al-Heety, A. J., Hassouneh, M., & Abdullah, F. M. (2021). Application of MASW and ERT methods for geotechnical site characterization: A case study for roads construction and infrastructure assessment in Abu Dhabi, UAE. *Journal of Applied Geophysics*, *193*, 104408.

Amin, M. M., Nasr, A. M. A. A., El-Bary, A. A., & Abo-Dahab, S. M. (2022). Propagation of surface waves in generalized thermoelastic media under influence of magnetic field and rotation and its applications in

engineering and geophysics. *Mechanics Based Design of Structures and Machines*, *50*(10), 3417-3440.

Anbazhagan, P., Parihar, A., & Rashmi, H. N. (2012). Review of correlations between SPT N and shear modulus: a new correlation applicable to any region. *Soil Dynamics and Earthquake Engineering*, *36*, 52-69.

Archie, G. E. (1942). The electrical resistivity log as an aid in determining some reservoir characteristics. *Transactions of the AIME*, *146*(01), 54-62.

Bajaj, K., & Anbazhagan, P. (2019). Seismic site classification and correlation between Vs and SPT-N for deep soil sites in Indo-Gangetic Basin. *Journal of Applied Geophysics*, *163*, 55-72.

Beck, Y. L., Palma Lopes, S., Ferber, V., & Côte, P. (2011). Microstructural interpretation of water content and dry density influence on the DC-electrical resistivity of a fine-grained soil. *Geotechnical Testing Journal*, *34*(6), 694-707.

Bertermann, D., & Schwarz, H. (2018). Bulk density and water content-dependent electrical resistivity analyses of different soil classes on a laboratory scale. *Environmental Earth Sciences*, *77*, 1-14.

Blanchy, G., Saneiyan, S., Boyd, J., McLachlan, P., & Binley, A. (2020). ResIPy, an intuitive open source software for complex geoelectrical inversion/modeling. *Computers & Geosciences*, *137*, 104423.

Braga, A. C. O., Malagutti F°_, W., Dourado, J. C., & Chang, H. K. (1999). Correlation of Electrical Resistivity and Induced Polarization Data with Geotechnical Survey Standard Penetration Test Measurements.

Journal of Environmental and Engineering Geophysics, *4*(2), 123–130. https://doi.org/10.4133/jeeg4.2.123

Butalia, T. S., Huang, J., Kim, D. G., & Croft, F. (2003). Effect of moisture content and pore water pressure buildup on resilient modulus of cohesive soils in Ohio. *ASTM Special Technical Publication*, *1437*(1), 70–84.

Chang, M., Kuo, C. P., Shau, S. H., & Hsu, R. E. (2011). Comparison of SPT-N-based analysis methods in evaluation of liquefaction potential during the 1999 Chi-chi earthquake in Taiwan. *Computers and Geotechnics*, *38*(3), 393-406.

Chu, Y., Liu, S., Bate, B., & Xu, L. (2018). Evaluation on expansive performance of the expansive soil using electrical responses. *Journal of Applied Geophysics*, *148*, 265-271.

Coelho, V. L., Piantini, A., Almaguer, H. A. D., Coelho, R. A., Boaventura, W. D. C., & Paulino, J. O. S. (2015). The influence of seasonal soil moisture on the behavior of soil resistivity and power distribution grounding systems. *Electric Power Systems Research*, *118*(1), 76–82. https://doi.org/10.1016/j.epsr.2014.07.027

Cosenza, P., Marmet, E., Rejiba, F., Jun Cui, Y., Tabbagh, A., & Charlery, Y. (2006). Correlations between geotechnical and electrical data: A case study at Garchy in France. *Journal of Applied Geophysics*, *60*(3–4), 165–178. https://doi.org/10.1016/j.jappgeo.2006.02.003

Dafalla, M. A., & AlFouzan, F. A. (2012). Influence of physical parameters and soil chemical composition on electrical resistivity: a guide for

geotechnical soil profiles. *International Journal of Electrochemical Science*, *7*(4), 3191-3204.

de Jong, S. M., Heijenk, R. A., Nijland, W., & van Der Meijde, M. (2020). Monitoring soil moisture dynamics using electrical resistivity tomography under homogeneous field conditions. *Sensors*, *20*(18), 5313.

Devi, A., Israil, M., Anbalagan, R., & Gupta, P. K. (2017). Subsurface soil characterization using geoelectrical and geotechnical investigations at a bridge site in Uttarakhand Himalayan region. *Journal of Applied Geophysics*, *144*, 78-85.

Dezert, T., Fargier, Y., Lopes, S. P., & Cote, P. (2019). Geophysical and geotechnical methods for fluvial levee investigation: A review. *Engineering Geology*, *260*, 105206.

Dick, M., Bery, A. A., Akingboye, A. S., & Gnapragasan, J. (2025). Integrated Machine Learning Modeling of Seismic , Electrical Resistivity , Induced Polarization , and SPT-N Data for Subsurface Integrity Assessment in Granitic Terrain. *Earth Systems and Environment*, *9*(3), 2457–2480. https://doi.org/10.1007/s41748-025-00772-2

Dikmen, Ü. (2009). Statistical correlations of shear wave velocity and penetration resistance for soils. *Journal of Geophysics and Engineering*, *6*(1), 61-72.

Drahor, M. G., Göktürkler, G., Berge, M. A., & Kurtulmuş, T. Ö. (2006). Application of electrical resistivity tomography technique for

investigation of landslides: a case from Turkey. *Environmental Geology*, *50*, 147-155.

Fatehnia, M., Hayden, M., & Landschoot, M. (2015). Correlation between shear wave velocity and SPT-N values for North Florida soils. *Electronic Journal of Geotechnical Engineering*, *20*(22), 12421-12430.

Fäth, J., Kunz, J., & Kneisel, C. (2022). Monitoring spatiotemporal soil moisture changes in the subsurface of forest sites using electrical resistivity tomography (ERT). *Journal of Forestry Research*, *33*(5), 1649-1662.

Gautam, D. (2017). Empirical correlation between uncorrected standard penetration resistance (N) and shear wave velocity (Vs) for Kathmandu Valley, Nepal. *Geomatics, Natural Hazards and Risk*, *8*(2), 496-508.

Goff, D., Lorenzo, J., & Hayashi, K. (2015, March). Resistivity and shear wave velocity as a predictive tool of sediment type in coastal levee foundation soils. In *Symposium on the Application of Geophysics to Engineering and Environmental Problems 2015* (pp. 167-176). Society of Exploration Geophysicists and Environment and Engineering Geophysical Society.

Gonçalves, J. T. D., Botelho, M. A. B., Machado, S. L., & Netto, L. G. (2021). Correlation between field electrical resistivity and geotechnical SPT blow counts at tropical soils in Brazil. *Environmental Challenges*, *5*, 100220.

Gunn, D. A., Chambers, J. E., Uhlemann, S., Wilkinson, P. B., Meldrum, P. I., Dijkstra, T. A., ... & Glendinning, S. (2015). Moisture monitoring in clay embankments using electrical resistivity tomography. *Construction and Building Materials*, *92*, 82-94.

Haile, N. S. (1968). Geosynclinal theory and the organizational pattern of the North-west Borneo Geosyncline. *Journal of the Geological Society*, *124*(4), 177–188.

Hall, R., & Breitfeld, H. T. (2017). Nature and demise of the Proto-South China Sea. *Bulletin of the Geological Society of Malaysia*, *63*(63), 61–76. https://doi.org/10.7186/bgsm63201703

Hassan, W., Qasim, M., Alshameri, B., Shahzad, A., Khalid, M. H., & Qamar, S. U. (2024). Geospatial intelligence in geotechnical engineering: a comprehensive investigation into SPT-N, soil types, and undrained shear strength for enhanced site characterization. *Bulletin of Engineering Geology and the Environment*, *83*(10), 380.

Hatta, K. A., & Syed Osman, S. B. A. (2015). Correlation of Electrical Resistivity and SPT-N Value from Standard Penetration Test (SPT) of Sandy Soil. *Applied Mechanics and Materials*, *785*, 702–706. https://doi.org/10.4028/www.scientific.net/amm.785.702

Hegde, A., & Anand, A. (2022). Resistivity Correlations with SPT-N and Shear Wave Velocity for Patna Soil in India. *Indian Geotechnical Journal*, *52*(1), 161–173. https://doi.org/10.1007/s40098-020-00492-6

Hossain, M. B., Roknuzzaman, M., & Rahman, M. M. (2022). Liquefaction potential evaluation by deterministic and probabilistic approaches. *Civil Engineering Journal*, *8*(7), 1459-1481.

Hossain, M. I. (2018). *Evaluation of undrained shear strength and soil classification from cone penetration test*. Louisiana State University and Agricultural & Mechanical College.

Hu, P., Heslop, D., Rossel, R. A. V., Roberts, A. P., & Zhao, X. (2020). Continental-scale magnetic properties of surficial Australian soils. *Earth-Science Reviews*, *203*, 103028.

Hunter, J. A., Crow, H. L., Stephenson, W. J., Pugin, A. J. M., Williams, R. A., Harris, J. B., & Woolery, E. W. (2022). Seismic site characterization with shear wave (SH) reflection and refraction methods. *Journal of Seismology*, *26*(4), 631-652.

Hussien, M. N., & Karray, M. (2015). Shear wave velocity as a geotechnical parameter: an overview. *Canadian Geotechnical Journal*, *53*(2), 252-272.

Hutchison, C. S. (2005). Chapter IV - The Kuching Zone. *Geology of North-West Borneo*, *1939*, 19–66.

Ijaz, N., Ijaz, Z., Zhou, N., Rehman, Z., Ijaz, H., Ijaz, A., & Hamza, M. (2025). Optimizing Subsurface Geotechnical Data Integration for Sustainable Building Infrastructure. *Buildings*, *15*(1), 140–159.

Ijaz, Z., Zhao, C., Ijaz, N., & Aashan, R. (2023). Statistical evaluation of multiple interpolation techniques for spatial mapping of highly variable geotechnical facets of soil in natural deposition. *Earth*

Science Informatics, 105–129. https://doi.org/10.1007/s12145-022-00924-2

Ijaz, Z., Zhao, C., Ijaz, N., Aashan, R., & Junaid, M. F. (2023). Geospatial modeling of heterogeneous geotechnical data using conventional and enhanced conception of modified Shepard method - based IDW algorithms : application and appraisal. *Bulletin of Engineering Geology and the Environment*, 1–21. https://doi.org/10.1007/s10064-023-03435-6

Imai, T., Fumoto, H., & Yokota, K. (1975, November). The relation of mechanical properties of soil to P-and S-wave velocities in Japan. In *Proceedings of 4th Japan Earthquake Engineering Symposium, Tokyo, Japan* (pp. 89-96).

Imai, T., & Tonoughi, K. (2021). Correlation of N value with S-wave velocity and shear modulus. In *Penetration Testing, volume 1* (pp. 67-72). Routledge.

Imai, T. (1977). P and S wave velocities of the ground in Japan. *Proc. 9th ICSMFE, Tokyo, 1977*, *2*, 257-260.

Islam, I., Ahmed, W., Rashid, M. U., Orakzai, A. U., & Ditta, A. (2020). Geophysical and geotechnical characterization of shallow subsurface soil: a case study of University of Peshawar and surrounding areas. *Arabian Journal of Geosciences*, *13*(18), 949.

Ismail, N. I., & Yaacob, W. Z. W. (2018). Application of electrical resistivity tomography (ERT) for slope failure investigation: A case study from Kuala Lumpur. *Jurnal Teknologi (Sciences & Engineering)*, *80*(5).

Kemna, A., Binley, A., Cassiani, G., Niederleithinger, E., Revil, A., Slater, L., & Zimmermann, E. (2012). An overview of the spectral induced polarization method for near-surface applications. *Near Surface Geophysics*, *10*(6), 453-468.

Lech, M., Skutnik, Z., Bajda, M., & Markowska-Lech, K. (2020). Applications of electrical resistivity surveys in solving selected geotechnical and environmental problems. *Applied Sciences*, *10*(7), 2263.

Lee, J. S., & Yoon, H. K. (2015). Theoretical relationship between elastic wave velocity and electrical resistivity. *Journal of Applied Geophysics*, *116*, 51-61.

Lee, S. H. H. (1990). Regression models of shear wave velocities in Taipei basin. *Journal of the Chinese Institute of Engineers*, *13*(5), 519-532.

Liu, S. Y., Du, Y. J., Han, L. H., & Gu, M. F. (2008). Experimental study on the electrical resistivity of soil-cement admixtures. *Environmental Geology*, *54*(6), 1227–1233. https://doi.org/10.1007/s00254-007-0905-5

Madon, M. (2005). Geological Setting of Sarawak. In *Geological of North West Borneo* (Issue June, pp. 19–66). https://www.researchgate.net/publication/304132933

Malehmir, A., Bastani, M., Krawczyk, C. M., Gurk, M., Ismail, N., Polom, U., & Perss, L. (2013). Geophysical assessment and geotechnical investigation of quick-clay landslides–a Swedish case study. *Near Surface Geophysics*, *11*(3), 341-352.

Mathew, M. J., Menier, D., Siddiqui, N., Kumar, S. G., & Authemayou, C.

(2016). Active tectonic deformation along rejuvenated faults in tropical Borneo: Inferences obtained from tectono-geomorphic evaluation. *Geomorphology*, *267*, 1–15. https://doi.org/10.1016/j.geomorph.2016.05.016

Mathew, M. J., Menier, D., Siddiqui, N., Ramkumar, M., Santosh, M., Kumar, S., & Hassaan, M. (2016). Drainage basin and topographic analysis of a tropical landscape: Insights into surface and tectonic processes in northern Borneo. *Journal of Asian Earth Sciences*, *124*, 14–27. https://doi.org/10.1016/j.jseaes.2016.04.016

Meju, M. A., Gallardo, L. A., & Mohamed, A. K. (2003). Evidence for correlation of electrical resistivity and seismic velocity in heterogeneous near-surface materials. *Geophysical research letters*, *30*(7).

Mohd, E. W., Sota, T., Joseph, J. K., Arifin, A., Jonathan, L., Yoshinori, M., & Katsutoshi, S. (2011). Soils and Vegetation Condition of natural forests and secondary fallow forests within Batang Ai national park boundary, Sarawak, Malaysia. *Kuroshio Science*, *5*(1), 67-76.

Nabilah, A. B., Ahmadi, R., Harith, N. S. H., Adnan, A., & Suhatril, M. (2023). Development of elastic design response spectra with emphasis on far-source earthquakes for low to moderate seismic region. *Asian Journal of Civil Engineering*, *24*(6), 1747-1760.

Najar, I. A., Ahmadi, R., Amuda, A. G., Mourad, R., Bendary, N. El, Ismail, I., Bakar, N. A., & Tang, S. (2025). Advancing soil-structure interaction (SSI): a comprehensive review of current practices, challenges, and future directions. *Journal of Infrastructure*

Preservation and Resilience, *6*(1), 1–25. https://doi.org/10.1186/s43065-025-00118-2

Najar, I. A., Ahmadi, R. B., Jamian, M. A. H., Hamza, H. B., Ahmad, A., & Sin, C. H. (2022). Site-Specific Ground Response Analysis using the Geotechnical Dataset in Moderate Seismicity Region. *International Journal of Mechanics*, *16*, 37–45. https://doi.org/10.46300/9104.2022.16.5

Naseem, A., Jalal, F. E., & Naseem, A. (2020). Predicting sandy-clayey soil properties using electrical resistivity testing. *Proceedings of the Institution of Civil Engineers-Geotechnical Engineering*, *173*(1), 21-29.

Oh, S., & Sun, C. G. (2008). Combined analysis of electrical resistivity and geotechnical SPT blow counts for the safety assessment of fill dam. *Environmental Geology*, *54*(1), 31–42. https://doi.org/10.1007/s00254-007-0790-y

Ohba, S., & Toriumi, I. (1970, December). Dynamic response characteristics of Osaka Plain. In *Proceedings of the annual meeting AIJ (in Japanese)* (Vol. 12).

Ohta, T., Hara, A., Niwa, M., & Sakano, T. (1972, July). Elastic shear moduli as estimated from N-value. In *Proc. 7th Ann. Convention of Japan Society of Soil Mechanics and Foundation Engineering* (pp. 265-268).

Okamoto, T., Kokusho, T., Yoshida, Y., & Kusuonoki, K. (1989, October). Comparison of surface versus subsurface wave source for P–S logging in sand layer. In *Proc. 44th Ann. Conf. JSCE* (Vol. 3, pp. 996-7).

Pozdnyakov, A. I., Pozdnyakova, L. A., & Karpachevskii, L. O. (2006). Relationship between water tension and electrical resistivity in soils.

Eurasian Soil Science, *39*(S1), S78–S83. https://doi.org/10.1134/s1064229306130138

Rezaei, S., Shooshpasha, I., & Rezaei, H. (2018). Empirical correlation between geotechnical and geophysical parameters in a landslide zone (Case study: Nargeschal landslide). *Earth Sciences Research Journal*, *22*(3), 195–204. https://doi.org/10.15446/esrj.v22n3.69491

Saad, R., Nawawi, M. N. M., & Mohamad, E. T. (2012). Groundwater detection in alluvium using 2-D electrical resistivity tomography (ERT). *Electronic Journal of Geotechnical Engineering*, *17*, 369–376.

Samouëlian, A., Cousin, I., Richard, G., Tabbagh, A., & Bruand, A. (2003). Electrical resistivity imaging for detecting soil cracking at the centimetric scale. *Soil Science Society of America Journal*, *67*(5), 1319-1326.

Samouëlian, A., Cousin, I., Tabbagh, A., Bruand, A., & Richard, G. (2005). Electrical resistivity survey in soil science: a review. *Soil and Tillage research*, *83*(2), 173-193.

Saneiyan, S., Ntarlagiannis, D., Werkema Jr, D. D., & Ustra, A. (2018). Geophysical methods for monitoring soil stabilization processes. *Journal of Applied Geophysics*, *148*, 234-244.

Seed, H. B., & Idriss, I. M. (1981, October). Evaluation of liquefaction potential sand deposits based on observation of performance in previous earthquakes. In *ASCE national convention (MO)* (pp. 481-544).

Seed, H. B., Tokimatsu, K., Harder, L. F., & Chung, R. M. (1985). Influence of SPT procedures in soil liquefaction resistance evaluations. *Journal*

of geotechnical engineering, *111*(12), 1425-1445.

Shah, A. A., Zhafri, M. N., Delson, J., & Navakanesh, B. (2018). Major strike-slip faults identified using satellite data in central borneo, SE Asia. *Geosciences (Switzerland)*, *8*(5), 1–21. https://doi.org/10.3390/geosciences8050156

Siddiqui, F. I., & Osman, S. B. A. B. S. (2013). Simple and multiple regression models for relationship between electrical resistivity and various soil properties for soil characterization. *Environmental Earth Sciences*, *70*(1), 259–267. https://doi.org/10.1007/s12665-012-2122-0

Snapp, M., Tucker-Kulesza, S., & Koehn, W. (2017). Electrical resisitivity of mechancially stablized earth wall backfill. *Journal of Applied Geophysics*, *141*, 98-106.

Soil Survey Staff 2006. Keys to Soil Taxonomy. 10th edition. US. Department of Agriculture and Natural Resources Conservation Service, Washington, D.C.

Solberg, I. L., Long, M., Baranwal, V. C., Gylland, A. S., & Rønning, J. S. (2016). Geophysical and geotechnical studies of geology and sediment properties at a quick-clay landslide site at Esp, Trondheim, Norway. *Engineering Geology*, *208*, 214-230.

Srivastava, S., Mukerjee, S., & Sastry, R. G. (2010). Regression based in-situ shear wave velocity estimation from electrical resistivity data. In *Indian geotechnical conference* (pp. 1-9).

Sudha, K., Israil, M., Mittal, S., & Rai, J. (2009). Soil characterization using electrical resistivity tomography and geotechnical investigations. *Journal of Applied Geophysics*, *67*(1), 74-79.

Sunny, A., Andy, A., Bery, A., Babatunde, M., Dick, M. D., Bala, G. A., & Ale, T. O. (2024). Surface – subsurface characterization via interfaced geophysical – geotechnical and optimized regression modeling. *Modeling Earth Systems and Environment*, *10*(4), 5121–5143. https://doi.org/10.1007/s40808-024-02054-8

Tarmizi, T., Saad, R., Muztaza, N. M., Ismail, N. A., Saidin, M. M., & Mohamad, E. T. (2016). Integration of SPT (N-Value), Mackintosh Probe (M-Value) and Resistivity values for soft soil assessment. *Jurnal Teknologi (Sciences & Engineering)*, *78*(8-6).

Tan, D. N. K. (1982). The Lubok Antu Melange, Lupar Valley, West Sarawak: a Lower Tertiary subduction complex. *Bulletin of the Geological Society of Malaysia*, *15*(15), 31–46. https://doi.org/10.7186/bgsm15198204

Teng, C. S. (2003). Classification and management of the steepland for agriculture in Sarawak.

Tjia, H. D. (1998). The Dulit triangle in Sarawak: a most striking example of detachment tectonics. *Bulletin of the Geological Society of Malaysia*, *42*(December), 95–100. https://doi.org/10.7186/bgsm42199809

Uma Maheswari, R., Boominathan, A., & Dodagoudar, G. R. (2010). Use of surface waves in statistical correlations of shear wave velocity and penetration resistance of Chennai soils. *Geotechnical and Geological Engineering*, *28*, 119-137.

Wair, B. R., DeJong, J. T., & Shantz, T. (2012). *Guidelines for estimation of shear wave velocity profiles*. Pacific Earthquake Engineering Research Center.

Wang, P., Zhao, M., Du, X., Liu, J., & Xu, C. (2018). Wind, wave and earthquake responses of offshore wind turbine on monopile foundation in clay. *Soil Dynamics and Earthquake Engineering*, *113*, 47-57.

Zhang, T., Liu, S., & Cai, G. (2018). Correlations between electrical resistivity and basic engineering property parameters for marine clays in Jiangsu, China. *Journal of Applied Geophysics*, *159*, 640–648. https://doi.org/10.1016/j.jappgeo.2018.10.012

Zhao, Q., Yan, Y., Zhu, Z., Carter, A., Clift, P. D., Hassan, M. H. A., ... & Aziz, J. H. A. (2021). Provenance study of the Lubok Antu Melange from the Lupar valley, West Sarawak, Borneo: Implications for the closure of eastern Meso-Tethys?. *Chemical Geology*, *581*, 120415.